Physics – Uspekhi **67** (3) 251 – 271 (2024)

REVIEWS OF TOPICAL PROBLEMS PACS numbers: 07.57.Pt, **76.30. – v,** 78.20.Ls

Development of laser spectroscopy of spin noise

G G Kozlov, I I Ryzhov, A V Kavokin, V S Zapasskii

DOI: https://doi.org/10.3367/UFNe.2023.05.039367

Contents

Abstract. The review is devoted to a new branch in magnetic resonance spectroscopy based on the optical detection of stochastic spin precession: laser spin noise spectroscopy (SNS). The SNS method, like EPR spectroscopy, makes it possible to study the energy structure of the magnetic states of the medium but does not imply excitation of regular spin precession and, due to the use of a laser-polarimetric signal detection channel, has a number of unique properties. In the review, we consider the specific information capabilities of the magnetic resonance noise technique and describe experiments demonstrating the efficiency of this approach for studying the energy-related and dynamic properties of spin subsystems in solid and gaseous paramagnets. Via the example of exciton-polariton condensate emission, we consider the specific features of polarization noise in secondary emission, including the case of unpolarized light. A rigorous theoretical description of the polarimetric spin noise signal formation is given based on the model of inelastic (Raman) light scattering by elementary angular momentum carriers.

G G Kozlov [(1,a)], **I I Ryzhov** [(1,b)], **A V Kavokin** [(1,2,c)], **V S Zapasskii** [(1,d)]
[(1)] St. Petersburg State University,
Universitetskaya naberezhnaya 7-9, 199034 St. Petersburg, Russian Federation
[(2)] Russian Quantum Center, Innovation Center Skolkovo,
Bol'shoi bul'var 30, str. 1, 121205 Moscow, Russian Federation
E-mail: [(a)] g.kozlov@spbu.ru, [(b)] i.ryzhov@spbu.ru,
[(c)] a.kavokin@soton.ac.uk, [(d)] vzap@rambler.ru

Received 23 January 2023, revised 19 April 2023
Uspekhi Fizicheskikh Nauk **194** (3) 268 – 290 (2024)
Translated by V L Derbov

Keywords: spin noise spectroscopy, spin fluctuation spectroscopy, electron paramagnetic resonance, polarimetry, exciton-polaritons

1. Introduction

The magnetic properties of matter are of great interest both for fundamental research and for its applications. An important role in the study of these properties is played by the spectroscopy of electron paramagnetic resonance (EPR) and nuclear magnetic resonance (NMR), spanning the frequency range of $10^4 - 10^{11}$ Hz and allowing the study of the magnetic energy structure of matter in the frequency region adjacent to the far IR range. In this spectral region, the energy spectrum of most physical objects demonstrates a dependence on the applied magnetic field — a fact that gave the name to this kind of spectroscopy. This dependence plays the key role in magnetic resonance spectroscopy, since the magnitude and configuration of the magnetic field can be controlled by the experimenter, which turns out to be extremely valuable in implementing and interpreting original experiments, as well as in numerous applications of the magnetic resonance effect.

In typical magnetic resonance spectroscopy experiments, a weak AC magnetic field $\mathbf{B}$ at a frequency of v is applied to the sample of interest placed in a DC magnetic field $\mathbf{B}_v \exp(-\mathrm{i}vt)$, and the sample response [1] to the AC field as a function of frequency v is observed. This response exhibits resonances at the frequencies of transitions between Zeeman energy levels, which provides information on the properties of

[1] Usually, this response is magnetization $\mathbf{M}(t)$ observed directly or indirectly.

the elementary magnetic moment carriers of the system studied. Since in the simplest case the sample magnetization response $\mathbf{M}(t) = \mathbf{M}_\nu \exp(-\mathrm{i}\nu t)$ is described by the magnetic susceptibility $\chi_\nu = \chi'_\nu + \mathrm{i}\chi''_\nu$, $\mathbf{M}_\nu = \chi_\nu \mathbf{B}_\nu$, it is possible to say that, in traditional experiments of magnetic resonance spectroscopy (EPR and NMR), the frequency dependence of the magnetic susceptibility χ_ν of the sample is observed, the resonances of which carry information of its energy structure in the magnetic field. In the present paper, we discuss an alternative method of obtaining such information possessing a number of new properties and capabilities.

The frequency dependence of the magnetic susceptibility is known to be related to the power spectrum of the magnetization *spontaneous noise* by the fluctuation-dissipation theorem [1]; therefore, the information obtained by the methods of standard magnetic resonance spectroscopy can be, in principle, obtained by recording the power spectrum of the spontaneous noise of magnetization. This possibility was probably first pointed out by F Bloch [1], who showed that the spectrum of the magnetic susceptibility of sample nuclei can be recorded by observing the noise of nuclear magnetization. Successful experiments on such nonperturbative[2] observation of the nuclear magnetization noise [2–4] have shown the viability of this experimental approach and demonstrated its capabilities [5, 6].

In the papers cited above (as well as in many others), the technique typical of EPR and NMR was used to observe magnetization noise. It is based on recording electric signals from an oscillatory circuit (resonator) containing the studied sample. In many cases, this allowed using the standard high-sensitivity instrumentation of NMR spectroscopy to observe the noise. However, this method is not the only possible one. In earlier Ref. [7], the possibility of observing spin noise by detecting the Faraday rotation (FR) fluctuations in a probe light passed through a paramagnet was studied. The method of spin noise spectroscopy (SNS) (also referred to in the Russian literature as spin fluctuation spectroscopy) based on this approach in many cases demonstrates unique capabilities. Along with classical magnetic resonance spectroscopy, it is now an important instrument for studying the structure of energy levels and the dynamics of elementary magnetic moment carriers of matter (see, e.g., reviews [8–12]).

The SNS method, which can be considered a variant of the optical detection of magnetic resonance [13], lies at the intersection of two directions of research in two different branches of physics, namely, light intensity fluctuation spectroscopy (IFS) from optics [14] and the magnetic resonance method from radio spectroscopy [15]. The combination of properties of these two different methods of study determines the specific features of the experimental approach considered. As mentioned above, the spin (magnetic) noise, whose spectrum corresponds to that of the system's magnetic susceptibility, is recorded in SNS as polarization fluctuation in the probe light beam, which determines the conceptual difference between SNS and the classical Zavoysky EPR method. In particular, the spin noise method does not imply system exposure to a high-frequency resonant perturbation, does not require magnetic polarization of the medium, and, as will be seen below, allows implementing high spatial resolution in all three coordinates. The SNS method has proven its effectiveness in studying the resonant magnetic susceptibility of nanoobjects (quantum wells, quantum dots) [16, 17] and for observing the nuclear relaxation dynamics [18, 19] and nonlinear phenomena in such systems [20]. At present, this technique is actively applied to study atomic systems [21], in one of which (sodium vapor) pioneering study [7] in this field was carried out and which serve as a perfect model subject for studying the capabilities of the SNS method. Thus, Refs [22, 23] demonstrated the possibility of using the noise technique to reveal the degree of inhomogeneous broadening in optical spectra, for which the spectral dip burning technique is commonly used. The presence of an optical channel in SNS provided this technique with additional informative capabilities that bring it closer to the methods of nonlinear optics [24]. The optical specific features of the method also made it possible to propose a double-beam scheme experiment that allows studying both time and spatial correlations in spin systems [25]. As was shown in Ref. [26], the SNS method allows observing not only the noise of the magnetization *vector* spectrally localized at the Larmor frequency but also the fluctuations described by a second-rank *tensor*, giving rise to a noise component at the doubled Larmor frequency (*alignment* noise). As to extending the scope of SNS objects, the possibility of applying SNS to classical objects of EPR spectroscopy, namely, to dielectric crystals activated with paramagnetic ions, was recently demonstrated [27].

Regardless of the large number of English language publications on SNS, there is only one review on the SNS theory [28] in domestic journals. Therefore, the present review containing a description of SNS experiments and their interpretation will be useful for the Russian reader interested in SNS.

The review is organized as follows. Section 2 presents basic knowledge on SNS and estimates of the noise polarimetric signal values. Section 3 describes SNS experiments demonstrating a variety of capabilities of this experimental approach. In Section 4, the noise signals observed in SNS are interpreted in terms of scattering theory; it is shown that SNS con be considered as the heterodyne detection of Raman scattering. In Section 5, the review content is briefly summarized and the prospects of further SNS development are outlined.

2. Basic spin noise spectroscopy

2.1 Setting up the experiment

The SNS experiment implies detecting the spin fluctuations (fluctuations in magnetization) of the medium via the noise of its Faraday rotation. The basic schematic diagram of the corresponding experiment is extremely simple. A linearly polarized light beam (referred to below as the *probe beam*) passes through the medium studied and is detected with a polarimetric detector, the output signal of which is digitized and mathematically processed (Fig. 1). A wavelength-tunable laser with a low level of excess noise, e.g., a diode or a ring titanium-sapphire laser, is conventionally used as a source *1* of CW monochromatic light. The linear polarization of the probe light and its azimuth is specified by the combination of optical elements *2* (e.g., a half-wave phase plate of a combination of a quarter-wave plate and a polarizer). A magnetic field created by an electromagnet *4* is applied to the sample *3*. Sometimes, a strong permanent magnet is used instead of an electromagnet (see, e.g., [29]), which makes it possible to change the field direction, preserving its magni-

[2] That is, with no excitation of the system by an AC magnetic field, needed in the conventional techniques.

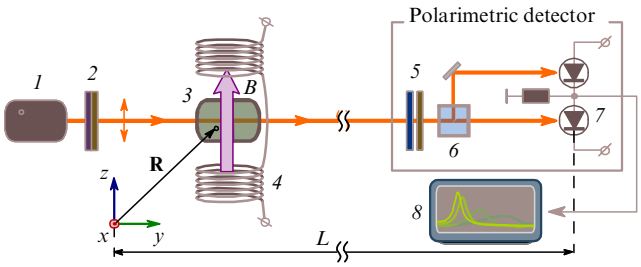

Figure 1. Schematic diagram of setup for observing spin noise. See text for element notation and explanation of operation principle.

tude. The light passed through the sample is directed to the polarimetric detector comprising phase plates *5*, a polarizing beam splitter *6*, and a differential (balanced) photodetector *7*. The output electric signal from the photodetector is determined by the difference among currents from photodiodes illuminated by the output beams from the polarizing beam splitter. In the balanced state, when the intensities of light in the arms of the polarizing beam splitter are equal, the mean output voltage of the polarimetric detector is zero. Before the measurements, the polarimetric detector, as a rule, is balanced so that its output signal is determined only by the *changes* in the polarization of the probe beam, caused by spin fluctuations in the sample. The output signal of the photodetector thus obtained arrives at the input of the digital radiofrequency spectrum analyzer *8*.

The phase plates *5* serve to balance the detector and switch between the modes of recording the noise of FR and ellipticity. When observing the FR fluctuations, the $\lambda/2$ plate used to balance the detector is installed before the beam splitter *6*. When observing the ellipticity fluctuations, a $\lambda/4$ plate oriented at 45° to the beam splitter polarizations is also installed before the beam splitter *7*, which allows converting the ellipticity changes into the rotations of the polarization pane registered by the polarimetric detector.

The change in the output voltage δU of the balanced polarimetric detector operating in the FR recording mode is proportional to the change $\delta\phi$ in the polarization azimuth of the incident light: $\delta U \sim \delta\phi$. If the sample contains magnetic particles (e.g., atoms or ions) and the projection of the magnetic moment of the ith particle on the propagation direction of the probe beam equals μ_i, then the linearly polarized probe beam experiences a rotation of the polarization plane by the angle $\delta\phi$ (Faraday effect), proportional to the total projection of the magnetic moment of the particles that find themselves inside the beam $\delta\phi = \kappa \sum_i \mu_i$, κ being the proportionality coefficient. If the magnetic moments composing the sample are oriented in space in a chaotic way, then the mean Faraday rotation of the probe beam polarization plane will be zero, $\langle\delta\phi\rangle = 0$; however, its mean square fluctuation $\langle\delta\phi^2\rangle$, the *Faraday rotation noise*, can differ from zero. The mean square fluctuation $\langle\delta U^2\rangle$ of the polarimetric detector output voltage will also be nonzero (see Fig. 1).

A magnetic field applied to paramagnetic material not only causes its magnetization but also radically changes the nature of its magnetization noise. This fact is of great informative value and forms the base of the spin noise spectroscopy method.

The mechanism of magnetic resonance noise signal formation can be presented in a simplified way as follows. If a transverse (with respect to the probe beam) magnetic field B is applied to the sample (see Fig. 1), then the magnetic moment of every particle of the sample will precess around it with the Larmor frequency $\Omega_L = g\beta B/\hbar$ (here, g is the g-factor, characterizing the particle, β is the Bohr magneton, $\hbar$ is the Planck constant), due to which the contribution of each particle to the total Faraday rotation $\delta\phi$ will oscillate at the same frequency. Since the phases of magnetic moment precession of the particles are random, the mean Faraday rotation will be zero again, $\langle\delta\phi\rangle = 0$. However, the power spectrum of its noise $\mathcal{N}(\nu)$ determined by the Fourier transform of the correlation function $\langle\delta\phi(0)\delta\phi(t)\rangle$ of the Faraday rotation $\mathcal{N}(\nu) = (2\pi)^{-1}\int \exp(i\nu t)\langle\delta\phi(0)\delta\phi(t)\rangle\, dt$ will exhibit a maximum[3] at the Larmor frequency Ω_L. This power spectrum (calculated instrumentally by the spectrum analyzer *8*) is the main result of measurements in SNS.

From the above consideration, it follows that, in the SNS experiment, the spectrum analyzer *8* actually records the spectrum of magnetization noise of the ensemble of sample particles that find themselves inside the probe beam.[4] As was already mentioned, according to the fluctuation-dissipation theorem [1], this spectrum is determined by the imaginary part of the sample magnetic susceptibility, which is detected in the standard EPR spectroscopy. This demonstrates the relationship between SNS and EPR spectroscopy, noted as far back as in Ref. [7].

From all of the above, it is obvious that the SNS technique reduces the problem of observing magnetization noise to the observation of the probe beam polarization noise. As a rule, the sensitivity of differential polarimeters used in SNS (see Fig. 1) is limited only by the shot noise of the probe beam [31] and, as follows from estimates presented below, turns out to be sufficient for reliable observation of the magnetization noise (spin noise) in many paramagnetic structures.

2.2 Estimating the signal value

To estimate the noise signal value, let us consider the following Gedankenexperiment. Let us apply to the sample a magnetic field parallel to the probe beam (i.e., in the y-axis direction in Fig. 1). Let the magnetic field be so strong that all elementary magnetic moments of the sample turn out to be oriented along it. Under equilibrium conditions, this means that the magnitudes of Zeeman splitting of magnetic energy sublevels of the system substantially exceed the thermal energy kT. In this case, a probe beam passed through such fully polarized sample will experience a rotation of the polarization plane ϕ_s, which we will call the *saturated rotation* and which, in principle, can be measured. We denote by N the number of particles contributing to this rotation.[5] The contribution of each particle $\delta\phi_i$ $(i = 1, \ldots, N)$ to the observed rotation ϕ_s will, in this case, be similar, since the magnetic moment projection on the probe beam direction is the same for all particles in the beam and has the maximum possible value. We denote it by μ. Therefore, the total

[3] From the relation presented, it is seen that the area under the noise power spectrum curve equals the mean square fluctuation of the Faraday rotation: $\int \mathcal{N}(\nu)\, d\nu = \langle\delta\phi^2\rangle$.

[4] This statement is valid when the Van Fleck theorem of proportionality between FR and magnetization holds. A more general case, when the relation between Faraday rotation of the probe beam and the medium magnetization is not scalar, is more thoroughly considered in Ref. [30].

[5] This is the number of particles that find themselves in the beam both spatially and spectrally, i.e., resonant to the probe beam (in the case of strong inhomogeneous broadening of the optical line, not all the particles geometrically inside the beam will make the same contribution).

recorded rotation ϕ_s can, in the considered case, be expressed by means of the proportionality coefficient κ introduced above as follows:

$$\phi_s = \sum_{i=1}^{N} \delta\phi_i = \kappa \sum_{i=1}^{N} \mu_i = N\kappa\mu\,.$$

Now, let us turn off the magnetic field and wait until the sample reaches a state of thermodynamic equilibrium. The observed rotation of the probe beam polarization plane $\delta\phi$ will be, as above, the sum of contributions from particles: $\delta\phi = \sum_{i=1}^{N} \delta\phi_i = \kappa \sum_{i=1}^{N} \mu_i$, in which the quantities $\delta\mu_i$ will be random with zero mean values, because the magnetic field aligning the magnetic moments is now absent. Direct calculation of the mean square fluctuation $\langle\delta\phi^2\rangle$ shows that $\langle\delta\phi^2\rangle = \kappa^2 N\langle\mu_1^2\rangle$. Here, $\langle\mu_1^2\rangle$ is the mean square of the magnetic moment of a certain particle, for instance, the first one (due to statistical equivalence, this value is independent of the particle number). Combining the expression for $\langle\delta\phi^2\rangle$ with the expression for ϕ_s and bearing in mind that $\langle\mu_1^2\rangle/\mu^2 \sim 1$, we arrive at the following relation between the saturated rotation and the mean square fluctuation of rotation in the absence of a strong polarizing field:

$$\langle\delta\phi^2\rangle \sim \frac{\phi_s^2}{N}\,. \tag{1}$$

Relation (1) can be applied to estimate the Faraday rotation noise in the SNS experiments, since the value of ϕ_s can be evaluated from the static Faraday rotation in the sample in relatively small magnetic fields (we denote it by ϕ_0), when $g\beta B \ll kT$ — in this case, $\phi_s \sim \phi_0\, kT/g\beta B$.

From Eqn (1), it is clearly seen that for SNS experiments it is advantageous (to a certain degree) to focus the probe beam. Indeed, as long as the focusing is not accompanied by optical nonlinearity, the saturated rotation ϕ_s is independent of whether the probe beam is focused or not. At the same time, the number N of particles in the beam decreases upon focusing, which leads to an increase in the value of $\langle\delta\phi^2\rangle$ (1) observed in SNS. It should be noted that the signal observed in SNS thus exhibits a sensitivity to the known Z-scan technique in the absence of any optical effects nonlinear in light power [9, 32] and, therefore, possesses a tomographic potential, considered in Section 3.6 in more detail.

To assess the possibility of detecting the spin noise in the noises of Faraday rotation $\langle\delta\phi^2\rangle$, let us compare the spectral density of these noises with the density of probe beam shot noise, unavoidably present at the output of a polarimetric detector (see Fig. 1). Let us first estimate the values of $\langle\delta\phi^2\rangle$ for a typical SNS object — a cell with alkali metal vapor 1 cm in size with a concentration of metal atoms $n = 10^{12}$ cm^{-3}. Let us perform the calculation for the case when the cell is probed with a nonfocused laser beam with a diameter of 3 mm and power $I = 5$ mW, the beam frequency being detuned from the frequency of atomic transition by 1–2 GHz, which is of the order of Doppler broadening. In this case, the cell remains transparent for the probe beam, and the absorption of light in the medium can be ignored. Since in the case considered the polarization noise is created by atoms whose magnetic moment precesses in the applied transverse magnetic field (see Fig. 1), the noise power spectrum will have a maximum at the precession frequency $\Omega_L = g\beta B/\hbar$, and the width of the maximum will be $\sim 1/T_2$ (T_2 being the time of spin transverse relaxation).

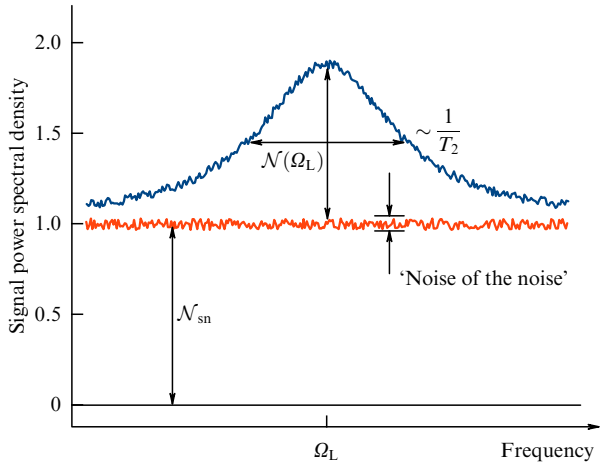

Figure 2. Schematic illustration of the signals observed in SNS.

Using the fact that the area under the noise spectrum curve $\int\mathcal{N}(\nu)\,d\nu = \langle\delta\phi^2\rangle$ can be estimated as $\mathcal{N}(\Omega_L)/T_2$, we get the following estimate for the noise power density at the precession frequency, where this density is maximum: $\mathcal{N}(\Omega_L) \sim \langle\delta\phi^2\rangle T_2 = \phi_s^2 T_2/N$. As shown in Ref. [31], for a polarimetric detector (see Fig. 1), the shot noise of photons is equivalent to fluctuations in the polarization azimuth of the input beam with a white spectrum whose density $\mathcal{N}_{sn}(\nu)$ is independent of frequency ν and determined by the relation $\mathcal{N}_{sn}(\nu) \sim \hbar\omega/I$ [rad^2 Hz^{-1}] (here, I and $\hbar\omega$ are the probe beam power [W] and the energy of its quantum [J], respectively). Thus, the ratio of the spin noise magnitude to the shot noise of the polarimetric detector can be estimated as follows:

$$\frac{\mathcal{N}(\Omega_L)}{\mathcal{N}_{sn}} \sim \frac{\phi_s^2 T_2}{N}\,\frac{I}{\hbar\omega}\,. \tag{2}$$

In the case under consideration, $T_2 \approx 10^{-5}$ s, saturated rotation $\phi_s \approx 1$, the number of atoms in the beam $N \approx 10^{12}$, and the photon production rate $I/\hbar\omega \approx 10^{17}$ s^{-1}. Therefore, $\mathcal{N}(\Omega_L)/\mathcal{N}_{sn} \approx 1$, from which it follows that the spin noise spectrum at the output of the spectrum analyzer will have a bell-shaped (Lorentzian) profile with a width of $1/T_2$, placed on a horizontal pedestal corresponding to the shot noise of the photodetector. The magnitudes of the bell and the pedestal in the example considered should be approximately equal, as shown in Fig. 2.

Note that the equal amplitudes of the spin and shot noise, playing in the described experiments the role of signal and noise, respectively, do not mean at all that the signal-to-noise ratio is of the order of unity, since the real noise that limits the possibility of observing spin fluctuations is determined by the stochastic fluctuations of the shot noise pedestal, rather than by the pedestal itself, i.e., by 'noise of the shot noise.' As is known [33], the accuracy of determining the white noise power in a bandwidth of γ with the measurement time τ is described by the factor $(\gamma\tau)^{-1/2}$. This factor, which is often a few orders of magnitude, allows measuring the spin noise on a substantially subshot scale. The paper by Forrester [34], written back in the pre-laser epoch, can serve as an outstanding example of observing informative light intensity noise (at a level of 10^{-4} of the shot noise). In a real experiment using a focused probe beam and the most favorable study subjects, the relative value of the spin component of the noise can reach hundreds of percent.

2.3 Calculating the magnetic moment correlation function

Let us now perform the simplest model calculation of the noise power spectrum $\mathcal{N}(\nu)$ recorded in SNS, when the magnetic moment of the particles is described by the effective spin 1/2.[6] As was mentioned above, this spectrum is determined by the correlation function $\mathcal{N}(\nu) = (2\pi)^{-1}\int \exp(\mathrm{i}\nu t)\langle\delta\phi(0)\delta\phi(t)\rangle\,\mathrm{d}t$ of the random polarimetric signal $\delta\phi$, which, in cases typical of SNS, can be considered the sum of contributions from N particles of the sample (atoms, ions) that find themselves within the probe beam: $\delta\phi = \sum_{i=1}^{N}\delta\phi_i = \kappa\sum_{i=1}^{N}\mu_i$. Bearing in mind the statistical independence and equivalence of the particles, as well as the fact that the contribution from each particle to the Faraday rotation polarimetric signal is determined by the projection of its magnetic moment on the direction of the probe beam (in the case considered — the direction of the y-axis), we obtain the following expression for the noise spectrum $\mathcal{N}(\nu)$:

$$\mathcal{N}(\nu) = \frac{\kappa^2}{2\pi}\int \exp(\mathrm{i}\nu t)\sum_{i,k=1}^{N}\langle\mu_i(t)\mu_k(0)\rangle\,\mathrm{d}t$$

$$\rightarrow \mathcal{N}(\nu) = \frac{N\kappa^2}{2\pi}\int \exp(\mathrm{i}\nu t)\langle S_y(t)S_y(0)\rangle\,\mathrm{d}t\,. \qquad (3)$$

Here, we ignored the mean values of the form $\langle\mu_i\rangle\langle\mu_k\rangle$, $i \neq k$, which play no essential role in SNS, and denoted as $S_y \equiv \mu_i$ the y-projection of the magnetic moment of an arbitrary (e.g., the ith) particle.

We will refer to the laboratory system of coordinates with the y-axis parallel to the probe beam as the K-system (see Fig. 1). Let us calculate the correlator $\langle S_y(t)S_y(0)\rangle$ for the case of an *tilted* magnetic field, when, in addition to the component B_z (shown in Fig. 1), there is a component B_y along the direction of the probe beam, and the total field $B = (B_y^2 + B_z^2)^{1/2}$ is tilted by angle $\phi = \arctan(B_y/B_z)$ with respect to the direction z of the laboratory K-system of coordinates.

Now, let us move to the coordinate system K', rotated by angle ϕ relative to the x-axis of the system K. In such a system, the magnetic field will have only a z-component $\mathbf{B} = (0,0,B) = (0,0,(B_y^2 + B_z^2)^{1/2})$. Magnetic moment projections in the K' system (we denote them by M_x, M_y, and M_z) satisfy the Bloch equations [35]

$$\begin{cases} \dot{M}_x = \Omega_{\mathrm{L}}M_y - \dfrac{M_x}{T_2} \\ \dot{M}_y = -\Omega_{\mathrm{L}}M_x - \dfrac{M_y}{T_2} \quad \text{at} \quad \Omega_{\mathrm{L}} \equiv \dfrac{\mu B}{\hbar} = \dfrac{\mu\sqrt{B_y^2 + B_z^2}}{\hbar}\,. \\ \dot{M}_z = \dfrac{M_{\mathrm{eq}} - M_z}{T_1} \end{cases} \qquad (4)$$

Here, $\mu \equiv g\beta$ determines the magnetic moment of the particle considered,[7] T_1 and T_2 are the longitudinal and transverse relaxation times, and $M_{\mathrm{eq}} = 0.5\mu\,\mathrm{th}\,[\mu B/2kT]$ is the thermodynamically equilibrium value of the particle magnetic moment projection on the magnetic field direction. The solution of these equations with given values of the projections $M_x(0), M_y(0), M_z(0)$ at $t = 0$ has the form

$$\begin{cases} M_x(t) = \exp\left(-\dfrac{t}{T_2}\right)\left[M_x(0)\cos(\Omega_{\mathrm{L}}t) - M_y(0)\sin(\Omega_{\mathrm{L}}t)\right], \\ M_y(t) = \exp\left(-\dfrac{t}{T_2}\right)\left[M_x(0)\sin(\Omega_{\mathrm{L}}t) + M_y(0)\cos(\Omega_{\mathrm{L}}t)\right], \\ M_z(t) = M_{\mathrm{eq}} + \left[M_z(0) - M_{\mathrm{eq}}\right]\exp\left(-\dfrac{t}{T_1}\right). \end{cases} \qquad (5)$$

The transition to the laboratory K-system of coordinates is implemented through the following transformation of the spin projections (rotation by an angle of $-\phi$):

$$\begin{pmatrix} S_x \\ S_y \\ S_z \end{pmatrix} = \begin{pmatrix} 1 & 0 & 0 \\ 0 & \cos\phi & -\sin\phi \\ 0 & \sin\phi & \cos\phi \end{pmatrix}\begin{pmatrix} M_x \\ M_y \\ M_z \end{pmatrix}, \qquad (6)$$

from which we obtain

$$\begin{aligned} \langle S_y(0)S_y(t)\rangle = {} & \langle M_y(0)M_y(t)\rangle\cos^2\phi \\ & + \langle M_z(0)M_z(t)\rangle\sin^2\phi \\ & + \langle M_y(0)M_z(t)\rangle\cos\phi\sin\phi \\ & - \langle M_z(0)M_y(t)\rangle\cos\phi\sin\phi\,. \end{aligned} \qquad (7)$$

Let us substitute the expressions for $M_y(t)$ and $M_z(t)$ from (5) into relations (7). In this case, average values will arise that have the form

$$\begin{matrix} \langle M_y^2(0)\rangle, & \langle M_z^2(0)\rangle, \\ \langle M_y(0)M_z(0)\rangle, & \langle M_y(0)M_x(0)\rangle\,. \end{matrix} \qquad (8)$$

They are thermodynamic averages of the operators of magnetic moment projections, the matrices of which $M_{x,y,z}$ are expressed in terms of Pauli matrices $M_{x,y,z} = \mu\sigma_{x,y,z}$. The averaging is performed in the K' system of coordinates with the equilibrium density matrix, in the present case, of the effective spin 1/2 that has the form

$$\rho_{\mathrm{eq}} = \frac{1}{Z}\begin{pmatrix} \exp\left(-\dfrac{\mu B}{2kT}\right) & 0 \\ 0 & \exp\left(\dfrac{\mu B}{2kT}\right) \end{pmatrix},$$

$$Z = \exp\left(-\frac{\mu B}{2kT}\right) + \exp\left(\frac{\mu B}{2kT}\right). \qquad (9)$$

When calculating the mean values of the form $\langle M_x(0)M_y(0)\rangle$, one should take into account that the Pauli matrices in the operators M_x and M_y do not commute, so that the mean value is calculated as $\langle M_x(0)M_y(0)\rangle = \mu^2\,\mathrm{Sp}\,\rho_{\mathrm{eq}}[\sigma_x\sigma_y + \sigma_y\sigma_x]/2$. Only those mean values diagonal with respect to the projections will be nonzero:

$$\langle M_y^2(0)\rangle = \langle M_z^2(0)\rangle = \frac{\mu^2}{4}\,, \qquad \langle M_{\mathrm{eq}}M_z(0)\rangle = M_{\mathrm{eq}}^2\,,$$

$$M_{\mathrm{eq}} = \frac{\mu}{2}\ \mathrm{th}\ \frac{\mu B}{2kT}\,, \qquad (10)$$

[6] In the case of arbitrary effective spin, the calculation is similar.

[7] Here, g is the g-factor of the particles considered and β is the Bohr magneton.

from which

$$\langle M_y(0)M_y(t)\rangle = \frac{\mu^2}{4}\,\exp\left(-\frac{|t|}{T_2}\right)\,\cos(\Omega_{\rm L}t)\,,$$
$$\langle M_z(0)M_z(t)\rangle = M_{\rm eq}^2 + \left[\frac{\mu^2}{4} - M_{\rm eq}^2\right]\,\exp\left(-\frac{|t|}{T_1}\right). \quad (11)$$

Here, we made use of the fact that correlators are even functions of time. Substituting these equations into (7) and calculating the noise power spectrum $\mathcal{N}(\nu)$ as a Fourier transform of the correlation function $\langle S_y(0)S_y(t)\rangle$, we obtain

$$\frac{\mathcal{N}(\nu)}{N\kappa^2} = \frac{T_2\,\mu^2\cos^2\phi}{8}\left[\mathcal{L}\big([\nu-\Omega_{\rm L}]T_2\big) + \mathcal{L}\big([\nu+\Omega_{\rm L}]T_2\big)\right] + \frac{T_1[\mu^2 - 4M_{\rm eq}^2]\sin^2\phi}{4}\,\mathcal{L}(\nu T_1) + \sin^2\phi M_{\rm eq}^2\,\delta(\nu)\,, \quad (12)$$

where the Lorentzian is $\mathcal{L}(x) \equiv [\pi(1+x^2)]^{-1}$. From expression (12), it is seen that, in an tilted magnetic field, the noise spectrum is *not monomodal* [9]: along with the Lorentz peak at the Larmor frequency $\Omega_{\rm L}$, a peak at the zero frequency appears with a width of $\sim 1/T_1$. Thus, the noise spectrum carries information not only about the *magnitude* of the magnetic field in which the sample is placed but also about the *orientation* of this field relative to the probe beam. This property can be useful when using the SNS technique in magnetometry.

As is seen from the above estimates, the observation of spin noise in alkali metal vapors with strong narrow lines of allowed optical transitions, in principle, requires no exotic instrumentation (low-noise amplifiers, complex algorithms of data processing, etc.). In particular, this is confirmed by the fact that the first experiment on SNS [7] was carried out using conventional electronics of that time. However, to apply the SNS technique to objects with less favorable magnetooptical characteristics, it became necessary to substantially modify the technique of noise signal acquisition and processing. Thus, the application of digital spectrum analyzers based on the fast Fourier transform instead of scanning-type spectrum analyzers allowed a radical increase in the sensitivity of the method [36–39]. As a result, the SNS method was successfully applied to study semiconductor structures and became a working tool in this important field of modern physics. A special place among the objects of SNS is occupied by paramagnets with inhomogeneously broadened optical transitions, in which the noise power can undergo immense growth under the conditions of resonance probing. The most striking example of this kind is dielectric crystals doped with rare earth ions. They will be considered in Section 3.3.

3. Experiments on spin noise spectroscopy

In the present section, we describe some SNS experiments demonstrating the capabilities of this technique. In pioneering experiment [7], which initiated SNS, the object of study was alkali metal vapors, but the technique became widespread after its application to solid state semiconductor media, which are of great interest for up-to-date photonics and microelectronics [36–40]. That is why we begin this section by describing experiments with semiconductor systems. The efficiency of applying the SNS method to them is due to their sufficiently high magnetooptical activity and the possibility of using microcavities that enhance the SNS technique sensitivity and lead to several specific effects.

Let us briefly recall the properties of semiconductor materials and microcavities based on them that are important for SNS. First, note that an intrinsic semiconductor probed in the transparency region should exhibit no noises of optical susceptibility observed in SNS, since they are mainly related to fluctuations in the populations of electron energy levels in the bands. These fluctuations are strongly suppressed in an intrinsic semiconductor: the valence band is completely filled, the conduction band is completely empty, and at low temperatures spontaneous interband transitions are practically excluded. Optical susceptibility fluctuations become possible in the case of partial population of the conduction band levels by electrons or when vacant energy levels (holes) occur in the valence band. Both can be implemented by doping the semiconductor sample or by its additional optical excitation in the absorption region (*optical doping*). For example, let the sample be doped by a shallow donor impurity, so that the elctrons from the impurity levels are thermally excited in the area of the conduction band, partially populating the energy levels of this band. In this case, the optical transitions from the valence band to the populated states of the conduction band become impossible due to the Pauli principle, and the optical susceptibility associated with such transitions decreases. Possible fluctuations in the distribution of impurity electrons over the conduction band levels (including their spin dynamics) cause fluctuations in optical susceptibility, which can be observed using the SNS method. A similar situation can be obtained by optically populating the levels of the sample conduction band. In both cases, the electrons that appeared in the conduction band of the semiconductor sample can be to a certain extent considered particles involved in the analysis in the above section, the concentration of these particles being controllable in a wide range by changing the impurity concentration or the intensity of the sample optical excitation.

The latest nanotechnologies allow manufacturing extremely thin layers of semiconductor materials (quantum wells, ensembles of quantum dots), which are intensely investigated by methods of traditional optical spectroscopy and reveal properties that are important for fundamental research and applications [41]. Spin noise spectroscopy can offer additional and, sometimes, unique facilities for studying such structures; however, their small thickness can complicate direct observation of the polarization noise. To overcome this difficulty, structures are grown where the studied part of the medium is located inside a microcavity (Fabry–Perot interferometer) formed by two closely spaced Bragg mirrors. Placing the studied layer in a microcavity is equivalent to an increase in the thickness of the studied part by Q times (Q being the cavity Q-factor). This increase is due to the multiple reflection of the probe beam from the resonator mirrors and, therefore, multiple passage of the probe beam through the structure part located between them. Note that, however, when recording the noise signals of Faraday rotation, in contrast to regular signals, the phenomenon of an effective increase of the medium length in the resonator has specific features. In SNS experiments, the dependence of the noise polarimetric signal $(\langle\delta\phi^2\rangle)^{1/2}$ on the sample length L usually turns out to be a square root one, since, as is shown in Section 2, $(\langle\delta\phi^2\rangle)^{1/2} = \kappa(N\langle\mu_{\rm I}^2\rangle)^{1/2} \sim \sqrt{L}$. From the qualitative point of view, such a dependence follows from the fact

that the contributions from different regions of the sample to the total fluctuation of Faraday rotation $\delta\phi$ are not correlated. It is important that, when using microcavities, one should expect a *linear* (stronger) dependence of the noise polarimetric signal amplitude on the effective sample length QL for the following reason. As noted above, the probe beam multiply reflected in the microcavity actually passes through the sample Q times. The time required for this multiple passage in the thin resonators used in SNS experiments is estimated as $\sim QL_{\text{res}}/c$, where L_{res} is the microcavity length, c is the speed of light. As a rule, this is much smaller than the period of Larmor precession of the sample spins. Therefore, the presence of a microcavity is equivalent to passing the probe beam through Q *similar* samples, whose contributions to the polarimetric signal are fully correlated. Note that the polarimetric noise from samples with a microcavity can be observed not only in the transmitted but also in the reflected beam.

Now, let us describe some particular studies of such systems, based on using microcavities and illustrating the capabilities of SNS.

3.1 Observation of nuclear spin relaxation and the optical Stark effect

First, let us dwell on one of the most effective applications of SNS for detecting internal fields arising in a semiconductor system under optical pumping. The studied nanostructure and a schematic diagram of this experiment are presented in Fig. 3. The noise signal was observed from the mirror interspace of the microcavity, which was a layer of *n*-doped GaAs. Protocol of the experiment were as follows. The frequency of a linearly polarized probe beam was set equal to the resonance frequency of a microcavity, and the noise spectrum of the Faraday rotation was observed in the reflected beam. The observed maximum in the spectrum of spin fluctuations corresponded to the Larmor precession frequency of the conduction band electrons in the applied magnetic field. Then, using a quarter-wave phase plate (see Fig. 3), a small ellipticity was imparted to the probe beam,

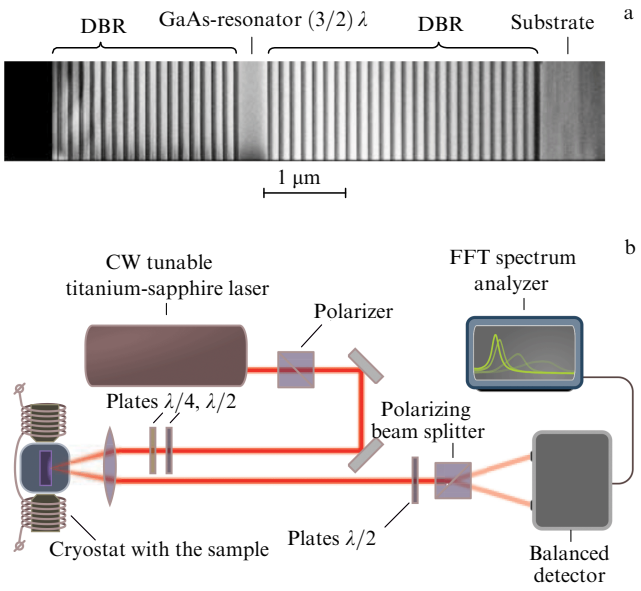

Figure 3. Observation of nuclear polarization and the optical Stark effect. The studied microcavity (a) and a schematic of the experiment (b). (Adopted from [19].)

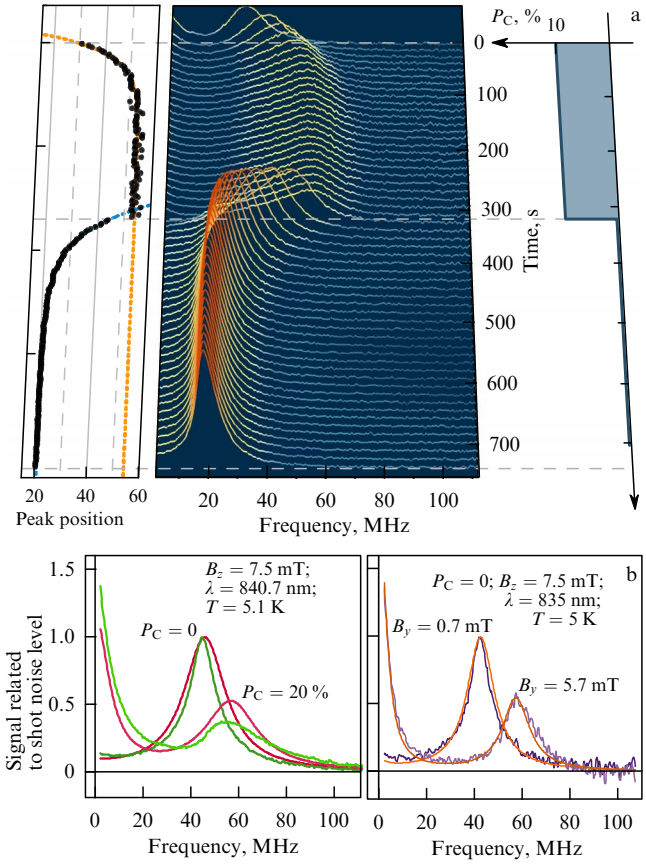

Figure 4. Observation of a self-induced effective magnetic field and dynamic polarization of nuclei in a layer of *n*-GaAs under the conditions of high density of probe light power. (a) Shift of the noise spectrum maximum upon increasing and decreasing the degree of light ellipticity. (b) Comparison of characteristic change in the shape of the spin noise spectrum upon increasing the ellipticity of the probe beam (left) and upon switching on an additional transverse magnetic field (right). The magnitude of the transverse magnetic field B_z is similar and constant in all experiments.

after which the frequency maximum of the noise spectrum shifted, the temporal dynamics of the shift having two components, a slow exponential one with a characteristic time of about 20 s and a second, virtually inertialess one. After 'switching off' the ellipticity of the probe beam, the noise spectrum returned to the initial state, demonstrating analogous dynamics (Fig. 4a).

The experiment could be interpreted [19] assuming that the slow component is due to the polarization of nuclei, induced by the elliptically polarized pumping light, and the inertialess one is due to the optical Stark effect. The known effect of optical orientation of nuclear spins [42] leads to an appearance of the effective magnetic field (Overhauser field) acting on the spins of the conduction band electrons and shifting the frequency maximum of the polarimetric noise associated with them. To orient the nuclei, a pump using light carrying angular momentum is required; therefore, the effect takes place only under elliptic polarization of the probe beam, which plays the role of pumping light. The characteristic times of the nuclear dynamics can be on the scale of tens of seconds, as was observed in the described experiment.

The phenomenology of the inertialess component of the noise spectrum dynamics corresponds to the so-called inverse Faraday effect [43, 44]. In Ref. [19], it was related to

renormalization of the Hamiltonian of electrons in a strong optical field; in the case of elliptic polarization of this field, the renormalization turns out to be equivalent to the action of an effective magnetic field (*'optical' field*) giving rise to additional splitting of spin levels and shifting the maximum of the noise spectrum. The 'optical' field is directed parallel to the probe beam, which is why in the experiments with transverse orientation of the static magnetic field (the Voigt geometry) the 'optical' field leads not only to a shift of the precession component of the noise spectrum but also to the appearance of a maximum at the zero frequency, analogous to the case of applying a certain tilted field (see Eqn (12) and Fig. 4b). Based on the results of Section 2.3, the value of the generated 'optical' field can be estimated in units of magnetic induction (see Fig. 4b).

Both effects described (optical orientation of nuclei and light-induced effective magnetic field) require sufficiently high density of the optical radiation and, therefore, most vividly manifest themselves in samples placed in a microcavity.

3.2 Information content of optical spectra of noise signals

One of the important features of SNS distinguishing it from classical EPR spectroscopy is the presence of an additional optical degree of freedom, the use of which substantially enriches the capabilities of studying spin systems. In the present section, we consider the specific features of the spin noise behavior under resonance probing of the medium and show that the dependence of spin fluctuation power on the frequency ω of the probe beam contains information on the character of the optical transition broadening unavailable for linear optics. This circumstance played an important role in the development of the SNS method and extending the scope of its attributes.

As was mentioned above, in cases typical of SNS, the recorded polarimetric signal $\delta\phi$ can be presented as the sum of contributions $\delta\phi_i$ from individual particles making up the samples studied, the contribution of the ith particle being proportional to its magnetic moment μ_i. Now, let us keep in mind that the proportionality coefficient (we denoted it by κ) can depend on the frequency of the probe beam ω and be different in different particles: $\delta\phi_i = \kappa_i(\omega)\mu_i$. If we ignore the contribution to the magnetooptical activity related to the frequency shift of the particle's energy levels in the magnetic field (the so-called A-term [45], which is usually small), then, within the simplest consideration, the particle may be characterized by one optical resonance frequency ω_0, $\omega_i \equiv \omega_0$. In this case, the frequency dependence $\kappa_i(\omega)$ has a dispersion-like form[8] and it turns out that $\delta\phi_i = a_i\mu_i[\omega_0 - \omega]/[(\omega_0 - \omega)^2 + \delta_i^2]$, where a_i is determined by the oscillator strength of the optical transition and δ_i characterizes its homogeneous width. It is natural to assume that the oscillator strength a_i and the homogeneous width δ_i do not fluctuate in time and in the first approximation are similar for all the particles, i.e., $a_i \to a$ and $\delta_i \to \delta$. The magnetic moment μ_i of each particle randomly precesses with the Larmor frequency Ω_L, as considered in detail above. As to the transition frequencies ω_i, three substantially different cases are possible.

(1) The spread of frequencies ω_i is smaller than the homogeneous width δ and we can assume that $\omega_i = \omega_0$ (*homogeneous broadening*).

(2) The frequencies ω_i are different in different particles and are constant in time (*static inhomogeneous broadening*).

(3) The frequencies ω_i are different and stochastically depend on time (*dynamic inhomogeneous broadening*).

The first two cases are implemented when the source of the spin noise are localized magnetic moments in solid-state matrices. At relatively high temperatures, the homogeneous broadening of optical transitions due to thermal vibrations of the crystal lattice is often prevalent. Upon decreasing the temperature, the homogeneous width decreases, and the static inhomogeneous broadening of spectra begins to play a role due to various kinds of inhomogeneities in the system. In some cases, e.g., in ensembles of quantum dots of semiconductor structures, the static inhomogeneous broadening has a morphologic nature and is the key factor of the optical spectrum formation. The third case is implemented mainly in classical SNS objects — alkali metal vapors — when the inhomogeneous broadening of the transition is determined by the Doppler effect.

As was already mentioned, due to the statistical equivalence of the sample particles, the noise power spectrum is determined by the Fourier transform of the correlator of the contribution from *one* (e.g., the first) particle $\mathcal{N}(\nu) = N[2\pi]^{-1}\int \exp(\mathrm{i}\nu t)\langle\delta\phi_1(t)\delta\phi_1(0)\rangle\,\mathrm{d}t$. In the simplest model, it is possible to consider $\mu_1(t)$ and $\omega_1(t)$ to be independent random processes and to perform 'uncoupling' when calculating the correlator $\langle\delta\phi_1(t)\delta\phi_1(0)\rangle$. Then, the correlator takes the form

$$\langle\delta\phi_1(t)\,\delta\phi_1(0)\rangle = a^2\langle\mu_1(t)\mu_1(0)\rangle \times \underbrace{\left\langle \frac{\omega_1(t)-\omega}{[\omega_1(t)-\omega]^2+\delta^2}\,\frac{\omega_1(0)-\omega}{[\omega_1(0)-\omega]^2+\delta^2}\right\rangle}_{D(t)}. \qquad (13)$$

The spin motion correlator $\langle\mu_1(t)\mu_1(0)\rangle$ was calculated above (see Eqns (3)–(12)) and in the simplest case $\langle\mu_1(t)\mu_1(0)\rangle = [\mu^2/4]\exp(-|t|/T_2)\cos(\Omega_L t)$. The correlator $D(t)$ (13) depends on which of the three cases mentioned above is realized in the experiment. In the simplest (first) case of homogeneous broadening, $\omega_1(t) = \omega_0 = \text{const}$, and we get

$$\langle\delta\phi_1(t)\delta\phi_1(0)\rangle = a^2\langle\mu_1(t)\mu_1(0)\rangle\left[\frac{\omega_0-\omega}{[\omega_0-\omega]^2+\delta^2}\right]^2. \qquad (14)$$

In the second case (static inhomogeneous broadening), the frequency $\omega_1(t)$ is independent of time, but random. Let us denote by $\rho_\Delta(\omega_1-\omega_0)$ its distribution function, which will be considered normalized, $\int\rho_\Delta(\omega_1-\omega_0)\,\mathrm{d}\omega_1 = 1$, having a characteristic width of Δ and centered at $\omega_1 = \omega_0$. In this case, the correlator $\langle\delta\phi_1(t)\delta\phi_1(0)\rangle$ is determined by the relation

$$\langle\delta\phi_1(t)\delta\phi_1(0)\rangle = a^2\langle\mu_1(t)\mu_1(0)\rangle \times\int\rho_\Delta(\omega_1-\omega_0)\left[\frac{\omega_1-\omega}{[\omega_1-\omega]^2+\delta^2}\right]^2\mathrm{d}\omega_1, \qquad (15)$$

which transforms into Eqn (14) at $\Delta \ll \delta$. At $\Delta \gg \delta$, the integral in Eqn (15) can be calculated using the fact that the contribution of the second term in square brackets is substantially nonzero only within a small domain $|\omega - \omega_1| \sim \delta$ and in fact behaves like $\pi\delta(\omega_1-\omega)/\delta$. There-

[8] If the Faraday rotation noise is recorded [45].

fore,

$$\left\langle \delta\phi_1(t)\delta\phi_1(0)\right\rangle = \frac{a^2\pi}{\delta}\left\langle \mu_1(t)\mu_1(0)\right\rangle \rho_{\Delta}(\omega-\omega_0)\,. \qquad (16)$$

From Eqn (16), it is seen that the optical spectral dependence of the noise signal in the case of inhomogeneous broadening practically reproduces the absorption profile $\sim \rho_{\Delta}(\omega-\omega_0)$ and substantially differs from zero in its center at $\omega=\omega_0$. This is qualitatively different from the case of homogeneous broadening when the spectral dependence of the noise signal (14) becomes zero in the center of the absorption profile at $\omega=\omega_0$. Thus, the observation of the optical spectral dependence of the noise signal in the SNS experiment offers a possibility of determining the character of broadening of the optical absorption line [22].

Consistent analysis of the third case (dynamic inhomogeneous broadening) requires specifying a model of atomic collisions; however, all results of importance for SNS can be obtained using the following simplified consideration. The observed frequency of the atomic resonance $\omega_1(t)$ differs from the atomic transition frequency ω_0 by the Doppler shift $\omega_1(t)=\omega_0+kv_y(t)$ (here, $k=\omega/c$, and $v_y(t)$ is the projection of atomic velocity onto the direction of the probe beam, which experiences random changes under interatomic collisions). The correlator $D(t=0)\equiv D_0$ can be calculated as

$$D_0=\int\left[\frac{\omega_0+kv-\omega}{\left[\omega_0+kv-\omega\right]^2+\delta^2}\right]^2\rho_{\mathrm{M}}(v)\,\mathrm{d}v\,. \qquad (17)$$

Here, $\rho_{\mathrm{M}}(v)=\left[v_T\sqrt{\pi}\right]^{-1}\exp\left(-[v/v_T]^2\right)$ is the Maxwell distribution (v_T being the mean thermal velocity of an atom). Let us denote by τ_{c} the mean time between the atomic collisions. Since during time $t<\tau_{\mathrm{c}}$ the change in the atom velocity is hardly probable, it is obvious that $D(t<\tau_{\mathrm{c}})\approx D_0$. At time $t\gg\tau_{\mathrm{c}}$, the velocities $v_y(t)$ and $v_y(0)$ become *independent* random quantities, having Maxwellian distribution functions. Therefore, the averaging of each of the factors (13) of the correlator $D(t)$ can in this case be performed independently, and we obtain

$$D(t\gg\tau_{\mathrm{c}})\equiv D_{\infty}=\left[\int\frac{\omega_0+kv-\omega}{\left[\omega_0+kv-\omega\right]^2+\delta^2}\,\rho_{\mathrm{M}}(v)\,\mathrm{d}v\right]^2. \qquad (18)$$

In order to calculate the correlator $D(t)$ at arbitrary time, it is possible to use the interpolation formula

$$D(t)=D_{\infty}+\left[D_0-D_{\infty}\right]\exp\left(-\frac{|t|}{\tau_{\mathrm{c}}}\right). \qquad (19)$$

It is now worth paying attention to the fact that at $\delta<kv_T$ the quantities D_0 and D_{∞} have substantially different dependences on the frequency ω of the probe beam. The argument analogous to that preceding Eqn (16) shows that D_0 approximately reproduces the absorption profile and reaches a maximum at $\omega=\omega_0$, whereas D_{∞} becomes zero in the center of the absorption profile at $\omega=\omega_0$ due to the evenness of the Maxwell distribution $\rho_{\mathrm{M}}(v)$.

Substituting Eqn (19) into (13) and performing the Fourier transform for the simplified spin correlator presented after Eqn (13), we conclude that the frequency dependence of the noise spectrum observed in SNS has the form[9]

$$\mathcal{N}(\nu)\sim D_{\infty}T_2L\left([\nu-\Omega_{\mathrm{L}}]T_2\right)+[D_0-D_{\infty}]\tau\,L\left([\nu-\Omega_{\mathrm{L}}]\tau\right), \qquad (20)$$

where $1/\tau\equiv 1/\tau_{\mathrm{c}}+1/T_2$.

In a real experiment with alkali metal vapors, the time between the collisions τ_{c} can be substantially smaller (in the presence of a buffer gas in the cell) or substantially larger (in its absence) than the spin relaxation time T_2. In the case of $T_2\ll\tau_{\mathrm{c}}$, the observed noise spectrum is determined by the expression $\mathcal{N}(\nu)\sim D_0T_2\,L([\nu-\Omega_{\mathrm{L}}]T_2)$ and depends on the probe beam frequency ω repeating the absorption profile and characteristic of an inhomogeneously broadened system. When $T_2\gg\tau,\tau_{\mathrm{c}}$, the noise spectrum recorded in the frequency window ν_s, such that $1/T_2<\nu_s<1/\tau_{\mathrm{c}}$, has the form $\mathcal{N}(\nu)\sim D_{\infty}T_2\,L([\nu-\Omega_{\mathrm{L}}]T_2)$ and at $\omega=\omega_0$ becomes zero as in the case of *homogeneous broadening* [22]. This effect of homogenization of the noise spectrum in an atomic system with *inhomogeneous* (Doppler) broadening was discovered and studied in Ref. [46]. Qualitatively, this homogenization effect can be considered to result from the fact that the spectrum of optical frequencies of each atom experiencing multiple collisions with atoms of buffer gas has enough time to fill practically the entire Doppler profile of the optical transition during time T_2.

3.3 Effect of giant amplification of spin noise in inhomogeneously broadened systems

The *optical spectroscopy* of spin noise, implying the dependence of spin fluctuation characteristics on the wavelength of the probe light, radically differs from common linear optical spectroscopy in its capabilities. The latter, as is known, is unable to determine the character of optical transition broadening, whereas the spin noise can differ in the most radical way not only in spectral but also in amplitude characteristics in cases of homogeneous and inhomogeneous broadening.

To estimate the value of the noise signal under conditions of resonant probing of the optical transition profile with mainly inhomogeneous broadening, we return to Eqn (1) relating the saturated Faraday rotation ϕ_s in the sample with the expected noise signal $\langle\delta\phi^2\rangle$. In this formula, the calculation of the number N of sample particles illuminated by the probe beam as nV (where n is the concentration of particles and V is the sample volume illuminated by the probe beam) is fraught with a strong underestimation of the noise signal $\langle\delta\phi^2\rangle$ due to the following reason. If the frequency ω of the probe beam hits within the inhomogeneously broadened absorption line, then the number of particles N entering Eqn (1) and contributing to the polarimetric signal can be substantially smaller than Vn, since this contribution is due to particles for which the detuning of their optical resonance from the probe beam frequency ω does not exceed the homogeneous width δ of this resonance. The number N of such 'resonant' particles can be estimated as $N\approx nV\delta/\Delta$ (here, Δ is the inhomogeneous width), after which Eqn (1) takes the form

$$\langle\delta\phi^2\rangle\sim\frac{\Delta}{\delta}\,\frac{\phi_s^2}{nV}\,. \qquad (21)$$

[9] For brevity, we do not write here the Lorentzians centered at negative frequencies (see Eqn (12)).

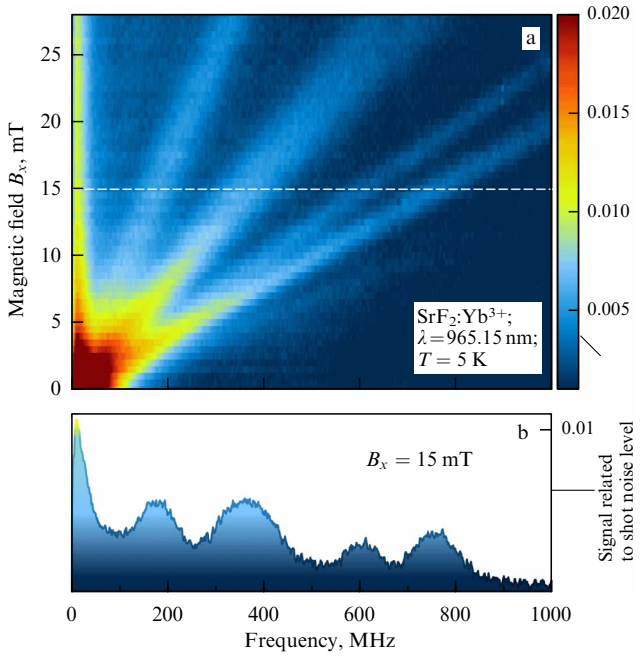

Figure 5. Dependence of spin fluctuation spectrum of the ytterbium ion in a strontium fluoride crystal on the magnitude of an applied transverse magnetic field (a) and one of the dependence spectra (b) (section position is indicated on color map by the dashed straight line). (Adopted from [27].)

Expression (21) shows that the samples with large relative inhomogeneous broadening Δ/δ can exhibit high-power noise signals and serve as good subjects for SNS even if their *regular* magnetooptical activity (ϕ_s) is not high. It is interesting that, in the case of forbidden optical transitions with extremely small values of homogeneous linewidths, such gain can be huge. Qualitatively, this can be explained by the fact that the loss in the noise signal related in this case to the small value of the saturated rotation ϕ_s is abundantly compensated for by the gain related to the huge value of the relative inhomogeneous broadening Δ/δ. This effect, called *giant spin noise amplification*, has been recently demonstrated experimentally [27] in some dielectric crystals with trivalent rare-earth ions. For parity-forbidden intraconfiguration (4f–4f) transitions in such ions, the ratio of inhomogeneous to homogeneous linewidth can reach 7–8 orders of magnitude, providing the appropriate gain in the value of the noise signal. The described effect allowed the first application of the spin noise technique to crystals with paramagnetic impurity centers and thus included them in the scope of SNS objects. Note that the preliminary studies carried out and estimates made [47] showed no prospect for using allowed interconfiguration (4f–5d) transitions in rare-earth ions that possess high magnetooptical activity as subjects for SNS.

As an illustration, Fig. 5 presents one of the first results of detecting magnetic resonance spectra by the method of spin noise spectroscopy in strontium fluoride crystals with Yb^{3+} impurity ions [27]. The spin precession signal was recorded under resonant probing of the sample at the frequency of the intraconfiguration f–f transition of the impurity ion. As a source of probe radiation, a ring titanium-sapphire laser capable of ensuring the required sufficiently narrow spectrum was used.

Successful experiments on detecting magnetic resonance in the spectrum of spin noise in crystals allowed expecting a possibility of applying SNS to these ions in glassy matrices, where the ratio of inhomogeneous widths of f–f transitions to the homogeneous ones can reach huge values. The chances for success in this case were obviously decreased by the large linewidths of magnetic resonance lines formed by chaotically oriented impurity centers differing in *g*-factors. In experiments with glassy matrices doped with neodymium and ytterbium ions, indeed, no Faraday rotation noises due to spin magnetization were detected. However, polarization fluctuations of a different nature not earlier observed were detected in the frequency region up to 1 GHz, which were characterized by a 'white' spectrum and manifested themselves as ellipticity noises rather than noises from the polarization plane rotation. The detected noise was attributed to the fluctuations of the structural environment of the impurity ions specific to glasses [48]. The results obtained demonstrated the applicability of polarization fluctuation spectroscopy for the study of the structural dynamics of disordered media, usually described within the model of double-well potentials.

3.4 Observing spin noise in birefringent media

The Faraday effect underlying the SNS method always determined, as was believed earlier, one of the most important requirements regarding the object of study — the condition of its optical isotropy (or, at least, isotropy in the plane perpendicular to the propagation direction of the probing light). The logic of this requirement seemed quite natural: the measurement of the *noises* of Faraday rotation implies the possibility of measuring the Faraday rotation itself, which is practically impossible in birefringent media. However, theoretical analysis of the problem has shown that this is not true and that the stochastic fluctuations of gyration or linear birefringence in strongly anisotropic media can be detected as successfully as in isotropic media. Qualitatively, the difference in the effect of linear birefringence on a regular and noisy gyration can be explained as follows. The effect of FR suppression by linear birefringence is observed at anisotropic medium distances exceeding or comparable to the thickness of the half-wave plate. For this reason, linear anisotropy of the medium by no means affects the spatially noncorrelated gyration (with zero correlation length). The authors of Ref. [49] presented a rigorous theoretical consideration of this problem and showed that strongly anisotropic optical crystals capable of affecting most radically the polarization of light passed through them turn out to be practically isotropic from the point of view of noise spectroscopy — the power of spin fluctuations exhibits no visible dependence on either the polarization state of the probe light or the direction of its propagation.

The success of [49] was also developed in application to semiconductor materials currently in demand — halogenide perovskites. Reference [50] reported a substantial suppression of Faraday rotation in an $MAPbI_3$ single crystal under the phase transition from the cubic to the low-temperature phase; however, in this case, the signals of Faraday rotation fluctuations were successfully detected, which, in combination with the rotating field technique, allowed investigating the anisotropy of the spin subsystem and detecting crystal twinning [51]. The presented results substantially extend the scope of SNS subjects and are of extreme importance for using the considered spectroscopic technique both in fundamental studies and in practical applications.

3.5 Alignment noise

In the above consideration, fluctuations in Faraday rotation or fluctuations of *gyrotropy* (circular birefringence) detected in SNS are a result of the fluctuating difference in the number of spins oriented parallel and antiparallel to the direction of probe light propagation. It is possible to say that the gyrotropy noise reflects the noise of spin *orientation*. The gyrotropy is described by the antisymmetric part of the polarizability tensor or by the gyration *vector* dual to it. Hence, in the standard SNS geometry, the fluctuations in the antisymmetric part of the polarizability tensor of the medium are recorded. From purely symmetry considerations, however, it is possible to hypothesize that a fluctuating anisotropy of the medium may arise as a result of a difference in the number of spins oriented across the light beam in two orthogonal directions, e.g., horizontal and vertical. Such fluctuations generally are not accompanied by fluctuations in magnetization and gyrotropy of the medium and manifest themselves as noises of the symmetric part of the medium polarizability or noises of linear birefringence. In atomic physics, this kind of spin ordering (regular or stochastic) is called *alignment*. In contrast to the noises of orientation, the noises of alignment are observed as noises of the ellipticity of light passed through the medium rather than as fluctuations in its polarization azimuth. Below in Section 4, where SNS is interpreted in terms of scattering theory, it is shown that such noise can be observed in a usual SNS setup, where the polarimetric detector operates in the mode of recording the ellipticity of the input beam. In the general case, the alignment noises are detected both at the Larmor frequency (Ω_L) and at the frequency of its second harmonic ($2\Omega_L$) [26].

In contrast to the orientation noises, alignment noises most vividly manifest themselves in the Faraday geometry, when the probing light beam propagates along the external magnetic field. Experimentally, the alignment noise was observed in [26] in cesium atomic vapor. Figure 6 illustrates the results obtained in this study. We emphasize that the presence of the second harmonic of the Larmor frequency in the alignment noise spectrum is not a manifestation of the studied system's nonlinearity. Therefore, the appearance of such noise should be considered in the experimental study of the nonlinear effect and constructing models to describe it.

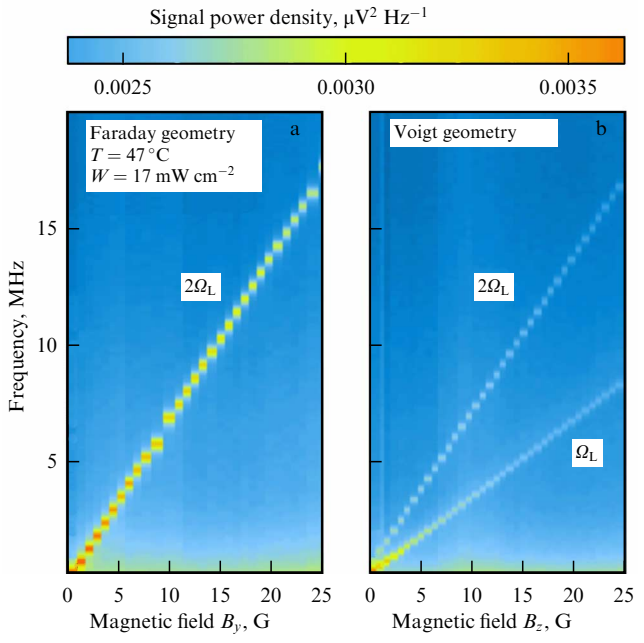

Figure 6. Dependence of ellipticity fluctuation spectra of cesium atoms on the magnitude of an applied magnetic field in Faraday (a) and Voigt (b) geometries.

3.6 Spin noise tomography

The technique uses the specific spatial locality of the noise signal recorded in SNS. As is known, the magnitude of the regular Faraday rotation (in linear optics) does not depend on the cross section of the probe beam. On the contrary, in SNS, where the stochastic rather than regular signal of Faraday rotation is measured, this is not true. As was already noted, as the cross section of the probe beam decreases (keeping its total power unchanged), the relative value of the spin fluctuation ($\sim 1/\sqrt{N}$) grows and, correspondingly, the value of the noise signal grows.

Therefore, for a focused Gaussian probe beam, the main contribution to the noise signal comes from the waist region, the length of which in the direction of beam propagation (Rayleigh length) is evaluated as ρ_c^2/λ (here, ρ_c is the waist radius, λ is the light wavelength). If the beam is formed by a fully illuminated lens with focal length f and diameter d, then at $\lambda \approx 1$ μm the radius of the beam waist ($\rho_c \approx \lambda f/d$) can be easily made to be a few microns and the Rayleigh length of the order of tens of microns. Moving the sample in such a beam and observing the noise signal, it is possible to measure the spatial distribution of spins that create the noise signal with the spatial resolution mentioned above. The described method of tomography was first demonstrated in [52] using the example of the depth spatial resolution of two n-GaAs layers of submillimeter thickness with different levels of doping. In Ref. [53], the spin noise spectroscopy of the gigahertz range was applied to study the relief of the electronic g-factor in bulk gallium arsenide near the crystal boundary. Thanks to using wide-aperture optics, the longitudinal spatial resolution reached in this study amounted to ~ 11 μm.

Note that the possibility of SNS-based three-dimensional tomography demonstrates again the closeness of SNS to the effects of nonlinear optics, since the dependence of the signal (in the present case, the noise signal) on the cross section of the beam (its intensity being constant) is nothing but a dependence of the signal on the density of light power, which is commonly direct evidence of optical nonlinearity.

3.7 Extending the frequency range of spin noise spectroscopy

Using optical detectors to record light intensity modulation signals at the Larmor frequency may seem to impose a substantial limitation on the frequency range of EPR spectroscopy measurements using the SNS method. However, this is not true. The simplest way to overcome such a limitation consists in using the method of signal heterodyning by intensity modulation. For this purpose, a probe beam is used with the intensity modulated at the frequency ν_T beyond the upper boundary of the detection range. In this case, a frequency shift of the noise spectrum occurs, $\mathcal{N}(\nu) \to \mathcal{N}(\nu - \nu_T)$, which allows it to be transfered to the frequency region available for observation. The method was first applied in Ref. [53], where, for the optical heterodyning, the radiation of a mode-locked laser was used. This radiation is a comb of short pulses, the repetition period of which $1/\nu_T$

substantially exceeds the duration of each pulse. Since the time dependence of the intensity of such radiation comprises multiple harmonics $nv_T, n = 1, 2, 3, \ldots$, the heterodyning in this case yields a series of shifted noise spectra $\mathcal{N}(v) \to \mathcal{N}(v - nv_T), n = \pm 1, \pm 2, \pm 3, \ldots$, which can be selected by moving the frequency window of the noise signal detection. In Ref. [53], using this method, it was possible to measure spin noise spectra in the range of a few GHz.

It is worth noting that a harmonic modulation of CW radiation can also be used as a heterodyne, implemented, e.g., by means of a Pockels cell and a high-frequency synthesizer. Another option is to use as a probe beam the mixed radiation of two stabilized CW lasers with frequencies detuned by v_T. Continuous frequency tuning of one of the sources in this case will allow measuring the frequency v_T and thus transfer the SNS signal from the frequency regions of tens or even hundreds of GHz, which can be used to measure Larmor frequencies in very strong magnetic fields or to study energy level splitting of a different origin.

The application of a probe beam with high-frequency modulation of intensity also allows realizing an interesting method of direct measurement of *time dependence* of the polarimetric noise correlation function in a range of extremely short times. Below, we present a simplified description of the method of optical observation of noise precession of spins at a frequency of ~ 30 GHz proposed in Ref. [54]. This frequency significantly exceeds the transmission band Δv_D of photodetectors and analog-to-digital converters (ADCs) used in SNS. The observation of the spin precession in Ref. [54] was implemented using ultrashort (with a duration of the order of hundreds of femtoseconds) laser pulses, repeated at a rate of $v_T \approx 100$ MHz. From such a sequence of pulses by means of a delay line (or using special laser systems), a sequence of pulse *pairs* was formed, separated by time interval Δt, which could be varied during experiments in the range from zero to hundreds of picoseconds. This sequence of pulse pairs was used to probe samples in the SNS scheme (Fig. 7), the transmission band of the photodetectors being $\Delta v_D \sim v_T \ll 1/\Delta t$.

Consider probing of the sample with the nth pair of optical pulses passed through the sample at times nT and $nT + \Delta t$, respectively. The output signal of the polarimetric detector δU will be determined by the Faraday rotation of the sample (or the magnetization $M(t)$ proportional to it) only at the moments nT and $nT + \Delta t$, when the sample is probed by the light. Since the transmission band of the photodetectors is relatively narrow, $\Delta v_D \ll 1/\Delta t$, the considered pair of optical pulses is not resolved in the output signal, due to which $\delta U \sim M(nT) + M(nT + \Delta t)$. According to the technique proposed in [54], the output signal δU was digitized, squared, and averaged:

$$\begin{aligned}\langle \delta U^2 \rangle &\sim \langle M^2(nT) \rangle + \langle M^2(nT + \Delta t) \rangle \\ &\quad + 2 \langle M(nT) M(nT + \Delta t) \rangle \\ &= 2 \langle M^2 \rangle + 2 \langle M(0) M(\Delta t) \rangle , \end{aligned} \tag{22}$$

and the obtained result was recorded as a function of the delay Δt between the pulses. As is seen from the presented relation, the part of $\langle \delta U^2 \rangle$ depending on Δt is proportional to the correlation function of magnetization $\langle M(0) M(\Delta t) \rangle$, the Fourier transform of which (magnetization noise power spectrum) is observed in the standard SNS experiments. Doped GaAs served as a sample in experiment [54], the delay time Δt was varied from zero to hundreds of picoseconds, and the function $\langle M(0) M(\Delta t) \rangle$ demonstrated oscillations with a period of about 100 ps, damping with the characteristic nanosecond time. Such behavior of the correlator $\langle M(0) M(\Delta t) \rangle$ corresponds to spin precession frequencies of the order of tens of gigahertz and a spin relaxation time of $\sim 10^{-9}$ s.

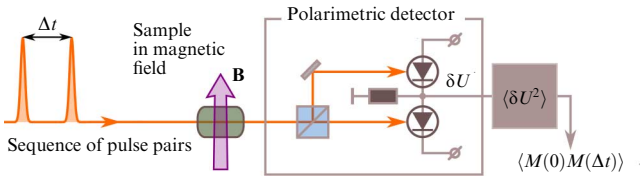

Figure 7. Schematic diagram of detecting spin precession in the microwave range significantly exceeding frequency band of polarimetric detector.

An interesting version of the development of the above technique is presented in Ref. [55], where a system of two independent pulsed mode-locked lasers was used for probing. The radiation from the lasers was combined into a single probe beam and passed through the sample to a standard polarimetric scheme, similar to that in Fig. 7. A minor difference in the pulse repetition rate ensures continuous 'scanning' of the delay δt between the pulses. The spectrum is reconstructed by means of the fast Fourier transform of the signal, which in this case is an autocorrelation function. Here, a registration bandwidth is reached that is determined by the value of δt^{-1} with the constant resolution $\delta t_{\max}{}^{-1}$, where $\delta t_{\max}$ is the maximum delay between the pulses. In Ref. [55], the detection bandwidth reached in this way amounted to more than 150 GHz.

3.8 Double-beam spin noise spectroscopy

In all the SNS experiments described above, the *frequency* spectrum of spin noise power was recorded, related to the *temporal* correlation function of spontaneous fluctuations of the sample magnetization. In Ref. [25], it was shown that, using the SNS method, it is, in principle, also possible to measure the *spatial* correlation function of the magnetization of the system studied, using an additional light beam coherent with the probing one and tilted with respect to it by the angle θ (Fig. 8).

As will be considered in more detail in Section 4, in SNS we actually observe the optical field *inelastically* scattered by the sample, the susceptibility of which experiences random fluctuations (Raman scattering of light). In the conventional geometry of the SNS experiment, this field acts on photodetectors together with the field of the probe beam and undergoes amplification due to the effect of heterodyning in quadratic photodetectors. It is important that the role of local oscillator in this experiment is played by the probe beam that gives rise to the scattered field. In the presence of an additional tilted beam scattered by the sample, an additional component appears, generated by the second beam. A part of this component hitting the aperture of the detector device is also heterodyned (the probe beam still serving as a local oscillator, since the tilted beam does not hit photodetectors) and contributes to the output signal of the polarimetric detector. As is shown in Ref. [25], this contribution naturally depends on the overlap of the probe and tilted beams in the sample region. However, the fact of primary importance is that, under certain conditions (in particular, when the size of the beam overlap region substantially exceeds the light wavelength $\lambda = 2\pi/k$), this contribution is proportional to

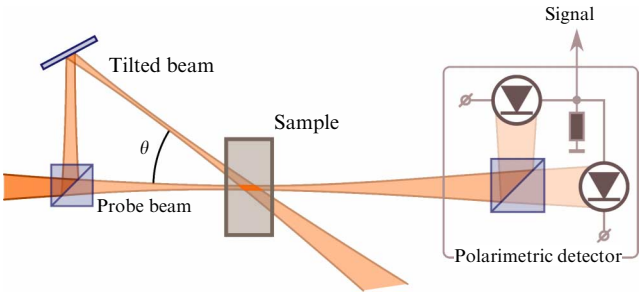

Figure 8. Double-beam SNS configuration.

the Fourier transform of the total *spatiotemporal* correlation function $\int \exp(\mathrm{i}[kr\sin\theta + vt])\langle M(0,0)M(\mathbf{r},t)\rangle\,\mathrm{d}t\,\mathrm{d}\mathbf{r}$ of the sample magnetization (gyrotropy). Thus, observing the contribution to the noise polarimetric signal related to the tilted beam at different angles θ, it is possible, in principle, to measure the total spatiotemporal correlator of the sample magnetization. The contribution of the tilted beam to the polarimetric signal of spin noise was detected in Ref. [56]. It is also worth mentioning Ref. [57], where an experimental technique analogous to that mentioned above was reported, in which the scattered field was mixed with the local oscillator field. The phase of the latter was controlled, which allowed monitoring not only the spin precession frequency but also the wave vector of the scattered light. As an example, a study of a layer of bulk *n*-doped CdTe was presented, for which the absence of spatial correlations was demonstrated.

Note that this double-beam heterodyning scheme can also be applied for high-sensitivity detection of *elastically* scattered light. In this case, the spectrum of the detected scattering signal turns out to be centered at the zero frequency, its width being determined by the dynamics of the medium's inhomogeneity. Since the intersection region of the two beams forming the signal can be made small enough, such a technique allows implementing not only high sensitivity to a weak inhomogeneity of the medium but also high spatial resolution in tomographic measurements. The advantages of this technique were experimentally demonstrated in Ref. [58].

3.9 Spin noise of a polariton laser and hidden polarization of nonpolarized light

Finally, let us consider a nonstandard option of SNS application: the detection of polarization fluctuations in the coherent light *emitted* rather than *scattered* by the object of study. To observe a signal in a 'classical' experimental setup, a reference beam is required, the role of which can be played either by light passing through the sample (standard scheme) or by a split external beam mixed with the scattered field (the so-called homodyne scheme [59]). However, the light emitted by any system can also be subjected to a similar procedure of polarimetric analysis. A trivial but, in practice, sought-after example is the analysis of polarization or intensity fluctuations of the radiation from a laser source, which allows determining the overall level of its excessive noises and the presence of sharp spectral features, related, e.g., to intermode beats. For this purpose, it is sufficient to direct the radiation of source *1* (see Fig. 1) exactly either to the balance polarimetric detector (to study the polarization noise) or to the single photodetector (to study the intensity noise). Much more in-depth results can be obtained when studying coherent radiation sources of a new type, the Bose–Einstein condensates of exciton polaritons, or polariton lasers, the radiation from which possesses hidden polarization even when on average it is not polarized. We consider this SNS application in a separate section, thus completing the review of SNS experiments by returning to semiconductor structures, since the existing polariton lasers are based on semiconductor microcavities.

Polarization characteristics of light are often described in terms of the Stokes vector (a vector on the Poincaré sphere), which allows assaying the predominant polarization of the beam or its absence. In the latter case, when all polarization components of the Stokes vector are zero, the light is considered unpolarized. Such light can be a result of averaging the light field polarization over time, spectrum, or in some other way; however, the Stokes vector contains no information about these details. Such a situation can be realized in practice, e.g., in the case of enhanced spontaneous emission, a superposition of many classical emitters, or the radiation from a polariton laser.

For light unpolarized on average, the distribution of Stokes vectors over the Poincaré sphere can be substantially different. Figure 9 presents several realizations of such 'unpolarized' sources: (a) linear emitters with random orientation of the polarization plane azimuth, (b) an equal number of right-hand and left-hand circularly polarized emitters, (c) a set of elliptic emitters with fixed orientation of the ellipse axes, (d) fully random emitters (truly unpolarized light). The above types of unpolarized radiation can be distinguished from each other by the character of polarization fluctuations. The hidden polarization character can be revealed by choosing a quarter-wave plate as *5* (see Fig. 1) and recording the integral noise signal depending on its orientation [60]. Figure 9e presents the corresponding theoretical dependences for the cases (a, b, d). When transmitting the light from the radiator with the distribution (a) through the quarter-wave plate, it becomes similar to the radiation with the distribution (c); therefore, it can be detected by rotating the balanced photodetector itself.

Thus, in some cases, it is possible to reveal the *hidden polarization* of the radiator, which can help in the interpretation of microscopic mechanisms of the formation of the radiating medium. We used this fact to study the polariton laser below and above the lasing threshold [61]. The radiation of polariton lasers is generated by an ensemble of exciton polariton quasiparticles formed in semiconductor heterostructures under the action of optical pumping [62] or direct electric injection [63]. The particles rapidly accumulate in one of the quantum states of the lower energy dispersion branch of exciton polaritons because of boson stimulation [64]. Due to this effect, the greater the number of particles already occupying this state, the higher the probability and, therefore, the rate of the transition to the state. The recombination of exciton polaritons from thus formed Bose condensate, the energy and wave vector of which are well defined, leads to the emission of light, possessing all characteristics of laser radiation: it is coherent, monochromatic, canalized, and polarized, at the same time remaining spontaneous. For SNS, these objects are of interest because theory predicts the appearance of giant polarization noise of the radiation [65]. The nature of this noise is related directly to the stochastic process of condensate formation, on the one hand, and to the bosonic stimulation effect, on the other hand. Moreover, as was shown in Ref. [66], the total polarization degree of the

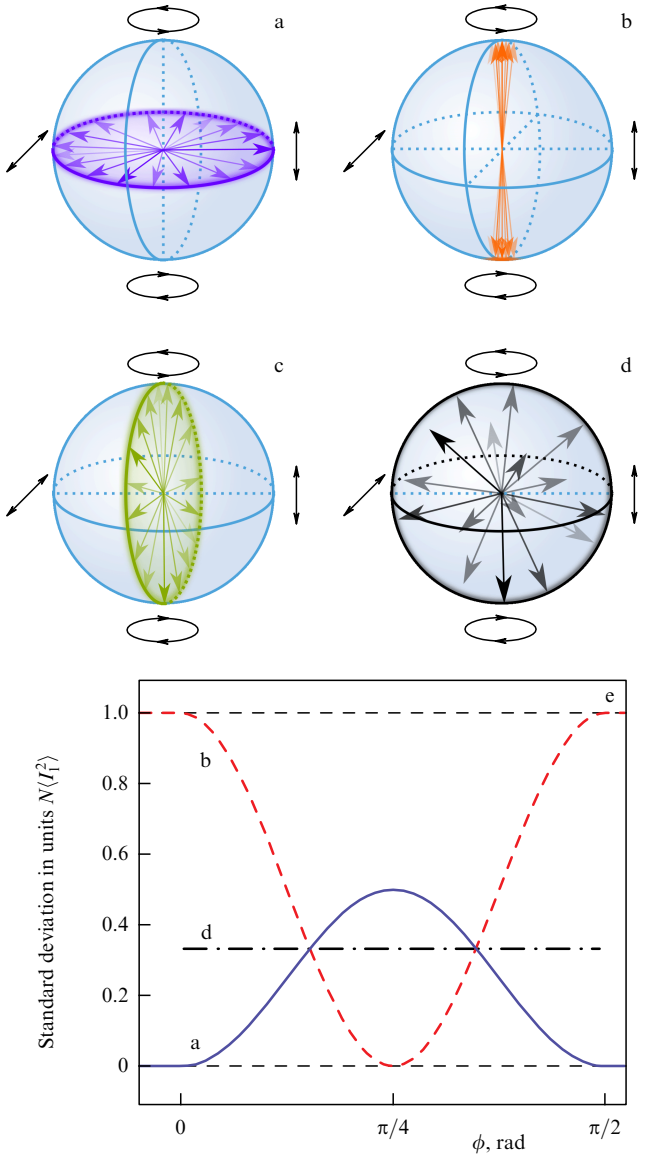

Figure 9. (a–d) Some special cases of distribution of individual emitters over the Poincaré sphere for light unpolarized on average. (e) Dependence on orientation of the quarter-wave plate before the detector for some distributions. See text for explanation.

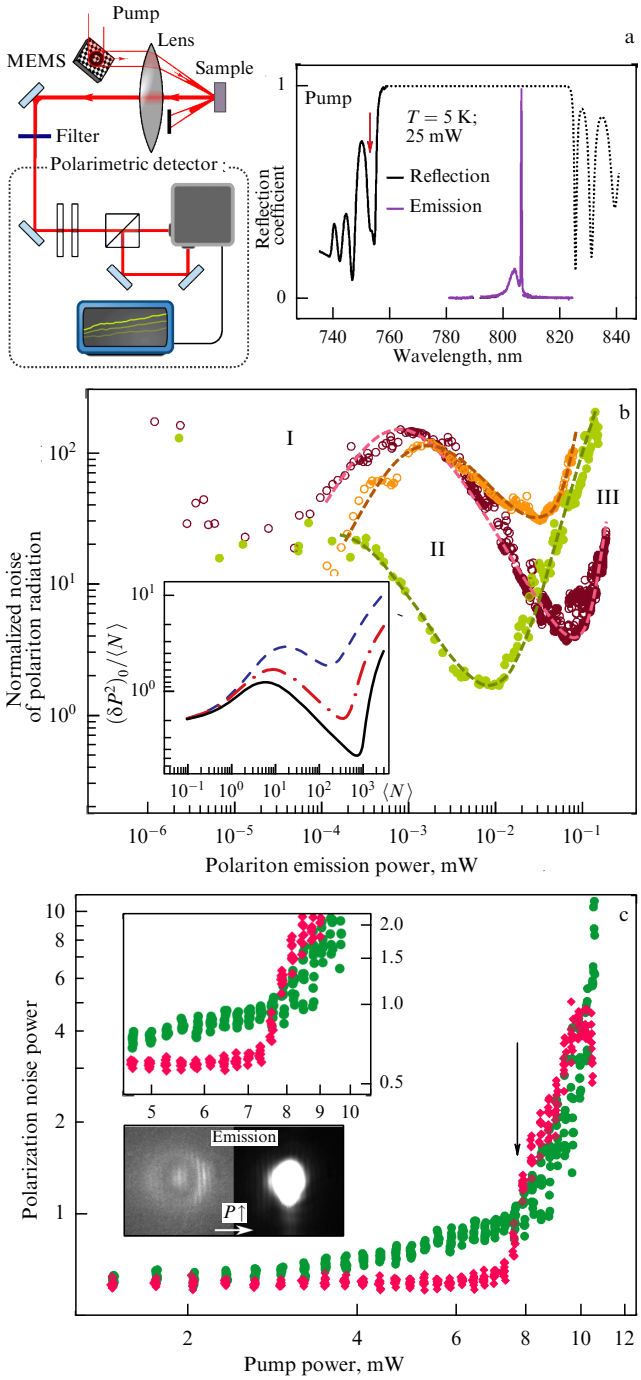

Figure 10. (a) Setup for recording the polariton-laser emission noise in from a polariton laser in an optical trap. (b) Dependence of the normalized integral of polarization plane rotation fluctuations of emitted light on its power (inset shows examples of the theoretical calculation of the dependence). (c) Dependence of the fluctuation integral of the polarization plane rotation (circles) and ellipticity (diamonds) on pump power in the case of a ring trap (inset shows a magnified detail of the dependence near the lasing threshold, indicated by an arrow).

polariton laser emission, i.e., the square root of the sum of squares of linear, diagonal, and circular polarization degrees, can be considered an order parameter of the transition from the incoherent gas of exciton polaritons to the Bose condensate. Thus, the formation of polariton condensate is always accompanied by a sharp growth of the polarization degree of light emitted by a microcavity. In the general case, the polarization of radiation from a polariton laser is random [64], but frequently it is pinned to one of the crystallographic axes [67]. Such a pinning can be caused by a slight optical anisotropy of Bragg mirrors forming the microcavity. When the pinning is absent, the polarization degree averaged over the time or the ensemble of exciting pulses can be close to zero, while its instantaneous total polarization can reach 80–90% [68]. Such unusual behavior of the emitted light polarization distinguishes the polariton laser from conventional semiconductor lasers. Spin noise spectroscopy is a method capable of revealing and characterizing this feature of the polariton laser [65].

As a sample, a high-Q microcavity was used based on GaAs containing four sets of three quantum wells located in the resonator antinodes [69]. Nonresonant pumping spectrally tuned above the mirror stop-band created a reservoir of hot excitons that then relaxed and emitted into the photonic mode of the resonator (see inset in Fig. 10a). The experiment is schematically presented in Fig. 10a. The pump *1* reflected from a micromechanical array of mirrors *2* was focused on the

sample *3* by the objective lens *4*. The light emitted by the sample along the direction of its epitaxial growth was filtered from the scattered pump light by the element *5* (e.g., a diffraction grating of a bandpass filter). Then, the beam was directed to the standard SNS scheme *6* to record the fluctuations in the polarization plane rotation.

First, a series of experiments has been carried out with a Gaussian profile of the pump beam, which yielded several important results. To being with, the radiation was indeed characterized by excess noises of polarization and intensity, exceeding by many times the level of shot noise. The observed power density spectrum of the fluctuations was 'white' in the frequency region available for detection under any conditions of experiment; therefore, the total signal was recorded in some limited frequency band (up to 100 MHz). This value was recorded depending on the power of pumping or emitted light, and the dynamic range of its variation turned out to be more than two orders of magnitude wider than the range of variation of the total light power,[10] which testifies to a very high sensitivity of the SNS technique to the changes in the studied polariton system. In addition, the dependence of normalized[11] fluctuations of the polarization plane rotation on the emitted light power turned out to be substantially nonmonotonic: first, the fluctuations grow (segment I in Fig. 10b), then decrease (segment II), and then grow again (segment III). The authors of Ref. [61] established the following proportionality of the fluctuations of polarization P normalized to the mean number of particles in the ground polariton state $\langle N \rangle$:

$$\frac{(\delta P^2)_0}{\langle N \rangle} \propto \frac{\langle N \rangle}{\Gamma_0 + |\alpha| \langle N \rangle^{3/2}}, \tag{23}$$

where Γ_0 is the rate of recombination of polaritons in the linear regime, and α is the effective constant of polariton-polariton interaction of polaritons with parallel spins, in turn, depending on the decay rate of the number of particles in the ground state (see [61]). In the initial segment I, the noise grows at the expense of decreasing the decay rate of fluctuations because of Bose stimulation and the corresponding decrease in the first term of the denominator in Eqn (23). When the polariton-polariton interaction increases, the second term begins to dominate in the denominator, and the normalized polarization noise decreases, which corresponds to segment II. The growth in the last segment III, apparently, testifies to the failure of the strong coupling mode and transition to the classical laser regime.

When the sample polariton laser is characterized by birefringence due to stresses or structure defects, the emitted light has some preferential polarization (thanks to the effect of polarization pinning mentioned above [67]). However, in the case of a high-quality structure and the absence of selected directions in it, the light can be practically fully depolarized in the static meaning, but characterized by polarization fluctuations, like those considered above. Indeed, in the experiment with such samples, it was found in [60] that the composition of their unpolarized radiation is close to a distribution of random emitters around the equator of the Poincaré sphere (Fig. 9a). These measurements were performed with a Gaussian shape of the pump beam.

By changing the spatial profile of the pump beam, one can create optical traps for the condensate due to the arising spatial gradient of the polariton energy — in the higher energy region, a blue shift of exciton polariton energy levels occurs, which leads to an accumulation of quasiparticles in the local minima of the potential. By varying the shape and size of such traps, one can substantially change the emission mode of the resulting condensate [71, 72]. In Ref. [73], using the SNS method, the dependences of fluctuations of polarization plane rotation and ellipticity of radiation from condensates in traps of various shapes were studied. The general and most significant feature of the observed signals (Fig. 10c) was their substantially different dependence on the pump power. The polarization plane rotation fluctuations arise in the radiation long before reaching the polariton lasing threshold (marked with an arrow), whereas the ellipticity fluctuations sharply arise after the threshold and significantly increase upon increasing the pump power, beginning to dominate over the rotation noises. The described effect can be interpreted as follows. In the unperturbed sample, there are small mechanical stresses due to the lattice mismatch of the materials forming the heterostructure. The magnitude of this anisotropy is insufficient to cause the pinning of the emitted light polarization; nevertheless, it suppresses the elliptic polarization of radiation and its fluctuations. An increase in the pump power beyond the threshold leads to a growth in $\langle N \rangle$ and an increase in the effective magnetic field arising due to spin-dependent polariton-polariton interactions [74]. Because of their strong spin anisotropy, the fluctuations of the population difference between the circularly polarized components of the condensate induce a rotation of its pseudospin. This effect is referred to as self-induced Larmor precession and is considered in detail in Ref. [73]. Note that, in terms of the distribution of emitters over the Poincaré sphere, this fact corresponds to a transition from configuration (a) at pre-threshold pump powers to distribution (b) above the threshold.

Thus, SNS is a method capable of revealing and characterizing the hidden polarization of radiation. This capability turns out to be of extreme importance for studies of a polariton laser. The method's sensitivity is particularly high in semiconductor microcavities with a high Q-factor, where the spin noise signal is amplified due to repeated circulation of light between the mirrors [16]. In particular, spin noise spectroscopy allows revealing the 'hidden' instantaneous polarization of the polariton condensate in those cases where the time-averaged polarization of the condensate is close to zero [60].

4. Spin noise spectroscopy from the point of view of scattering theory

4.1 Expression for the signal recorded in spin noise spectroscopy

In the above sections, when describing SNS experiments and performing numerical estimates, we implicitly assumed that the studied sample can be considered a homogeneous *rotator*[12]

[10] In experiments studying polariton lasers, the plot of emitted versus pump power is often used to determine the lasing threshold position (see, e.g., [70]).

[11] When measuring the spin noise spectra of light with variable intensity, it is almost always reasonable to normalize the result to the power of the beam incident on the detector, since this allows a direct comparison of the measurement results, while excluding from consideration the pedestal of the shot noise of light, which always linearly depends on the light intensity on the detector.

[12] That is, a part of the homogeneous medium possessing circular birefringence or gyrotropy.

that rotates the polarization plane of the probe beam through a random angle $\delta\phi$, representable as a sum of contributions from N particles of the sample that find themselves within the probe beam: $\delta\phi = \sum_{i=1}^{N} \delta\phi_i$, $\delta\phi_i \equiv \kappa\mu_i$ (see Section 2). Such an assumption needs to be substantiated, since the noise signals observed in SNS are generally a result of s*cattering* of the probe beam by the sample, whose optical susceptibility is inhomogeneous in space and fluctuates in time. Let us clarify the mechanism of forming the noise signals in SNS from this point of view.

In SNS, we observe fluctuations of the optical susceptibility caused by the random precession of magnetic moments of sample particles at the Larmor frequency $\Omega_L = g\beta B/\hbar$ and giving rise to components with frequencies $\omega \pm \Omega_L$ in the spectrum of the scattered radiation (spin flip Raman scattering effect). In the relevant case of weak scattering, the optical field at the input of the polarimetric detector (see Fig. 1) can be considered a sum of the probe beam field and the scattered field. The interference of the probe field and the components of the scattered field frequency-shifted by $\pm\Omega_L$ are accompanied by beats of intensity at the frequency Ω_L (effect of heterodyning). The effect gives rise to a spectral component at the frequency Ω_L [13] in the output current of photodetectors *7*, which is recorded as SNS polarimetric noise spectrally localized at this frequency. Note that, to observe these beats, it is necessary to install a polarizing beam splitter *6* before the photodetectors (see Fig. 1), since the intensity beats occur only due to the interference of similarly polarized fields and, as we will see below, the polarization of the scattered and the probing fields can be different. From the presented consideration, it is seen that SNS is, in essence, a heterodyne registration of Raman scattering, as was pointed out in Ref. [75].

Before proceeding to the calculation of the scattered field discussed above, let us describe a quantitative model of a polarimetric detector in Fig. 1 and present expressions for calculating its output signal. We will consider the case where the polarimetric detector operates in the mode of Faraday rotation recording (i.e., *5* is a half-wave phase plate). Let us introduce the coordinate system with the z-axis directed along the magnetic field (the Voigt geometry), the y-axis parallel to the probe beam (see Fig. 1), and the zx-plane parallel to the planes of photosensitive surfaces of photodetectors *7*. The principal directions of the polarizing beam splitter *6* are rotated by the angle ϕ with respect to the axes z and x of the above coordinate system. [14] Let us denote by $\mathbf{E}$ the complex optical field which *would* act on the lower (upper) photodetector if the polarizing beam splitter *6* is removed from the detector (replaced with a mirror directing the radiation to the upper photodetector); only the real part of $\mathbf{E}$ which will be denoted by the calligraphic character $\boldsymbol{\mathcal{E}} \equiv \mathrm{Re}\,\mathbf{E}$ will be considered to have physical meaning. Then, the photocurrent, e.g., of the lower photodetector, to a factor inessential for us here, is determined by the following integral:

$$T^{-1}\int_0^T \mathrm{d}t \int_S \mathrm{d}x\,\mathrm{d}z\,\mathcal{E}^2\,,$$

where S is the photosensitive surface of the photodetector, and the averaging over time t is performed in the interval T containing a large number of optical periods $2\pi/\omega$ and small compared to the characteristic time of the polarimetric signal change — in our case, the period of Larmor precession: $2\pi/\omega \ll T \ll 2\pi/\Omega_L$. Due to the presence of the polarizing beam splitter *7* in the scheme, each of the photodetectors is hit by one of the projections $\mathcal{E}_{x,z}$ of the field $\boldsymbol{\mathcal{E}}$ introduced above, and, due to the bridge connection of the photodetectors, the output signal U is determined by the differences in their photocurrents. Bearing all this in mind, we can derive the following expression for the signal U:

$$U = \frac{1}{T}\int_0^T \mathrm{d}t \int_S \mathrm{d}x\,\mathrm{d}z\left[\cos[2\phi](\mathcal{E}_x^2 - \mathcal{E}_z^2) - 2\sin[2\phi]\mathcal{E}_z\mathcal{E}_x\right], \tag{24}$$

where $\mathcal{E}_{x,z} \equiv \mathrm{Re}\,E_{x,z}$.

In correspondence with what is stated above, the complex field $\mathbf{E}$ can be presented as $\mathbf{E} = \mathbf{E}_0 + \mathbf{E}_1$, where $\mathbf{E}_0$ is the field of the probe beam and $\mathbf{E}_1$ is the field scattered by the sample. In SNS experiments, only part δU of the output signal of the polarimetric detector proportional to $\mathbf{E}_1$ is recorded. For this part, using Eqn (24), it is possible to obtain the expression

$$\delta U = \frac{2}{T}\int_0^T \mathrm{d}t \int_S \mathrm{d}x\,\mathrm{d}z\left\{\cos[2\phi](\mathcal{E}_{0x}\mathcal{E}_{1x} - \mathcal{E}_{0z}\mathcal{E}_{1z}) - \sin[2\phi](\mathcal{E}_{0x}\mathcal{E}_{1z} + \mathcal{E}_{0z}\mathcal{E}_{1x})\right\}, \tag{25}$$

where $\mathcal{E}_{0x,z} \equiv \mathrm{Re}\,E_{0x,z}$ and $\mathcal{E}_{1x,z} \equiv \mathrm{Re}\,E_{1x,z}$. Let us proceed to the calculation of the scattered field $\mathbf{E}_1$ entering this expression.

4.2 Calculating the scattered field

We will carry out a calculation of the scattered field $\mathbf{E}_1$ under the following simplifying assumptions:

(i) the polarimetric noise observed in SNS experiments is produced by an ensemble of some particles (atoms, ions) that find themselves within the probe beam;

(ii) the optical field acting on each particle can be considered equal to the field of the probe beam, which is assumed to be known (the approximation of single scattering and absence of self-action);

(iii) the optical response of each particle can be calculated in the linear approximation.

With the above assumptions, the calculation of δU reduces to determining the contribution to the polarimetric signal from *one* particle and summing over all particles located inside the probe beam. Let us find the field scattered by one particle (keeping for it the notation $\mathbf{E}_1$) and calculate using (25) the contribution δu_r of this particle to the polarimetric signal. Let the particle have the radius vector $\mathbf{R}$ (see Fig. 1) and be a point dipole executing forced oscillations in the field of the probe beam $\mathbf{E}_0$. The polarization distribution created by such a particle in space has the form

$$\mathbf{P}(\mathbf{r}) = \delta(\mathbf{R}-\mathbf{r})\begin{pmatrix}\langle d_x\rangle\\ \langle d_y\rangle\\ \langle d_z\rangle\end{pmatrix}\exp(-\mathrm{i}\omega t)\,, \tag{26}$$

where $\langle d_{x,y,z}\rangle$ are the projections of the dipole moment oscillation amplitudes for the considered particle. The desired field $\mathbf{E}_1$ is the radiation field of a point dipole and

[13] Since the photodetectors *7* of the polarimetric detector are quadratic, their output current is proportional to the intensity of the field on the photosensitive surface.

[14] With fixed polarization beamsplitter *6*, the angle ϕ can be changed by rotating the phase plate *5*, which in this case is a half-wave one.

can be found by solving the inhomogeneous Helmholtz equation

$$\Delta \mathbf{E}_1 + k^2 \mathbf{E}_1 = -4\pi k^2 \mathbf{P}, \quad k \equiv \frac{\omega}{c}. \tag{27}$$

Since we are interested in the radiation of the particles in the direction of the y-axis (the sample is displaced with respect to the polarimetric detector exactly in this direction; see Fig. 1), we omitted on the right-hand side of Eqn (27) the term $-4\pi\nabla\mathrm{div}\,\mathbf{P}$ — direct verification shows that, for the considered geometry of detection of the scattered radiation field $\mathbf{E}_1$, it is negligible.[15] For the same reason, it is possible to omit the component $\langle d_y \rangle$, since the dipole radiation in the direction of the y-axis is related only to the components orthogonal to this axis.

Equation (27) is derived assuming that the time dependence of all involved fields is harmonic, $\sim \exp(-\mathrm{i}\omega t)$. We will also use this equation when the oscillation *amplitude* of the polarization field $\mathbf{P}(\mathbf{r})$ experiences slow (compared to the frequency of optical oscillations ω) modulation at the frequency of spin precession $\Omega_\mathrm{L} \ll \omega$. The solution to Eqn (27) can be obtained using the Green's function of the Helmholtz operator $\Gamma(\mathbf{r}) = -\exp(\mathrm{i}kr)/4\pi r$, satisfying the equation $\Delta\Gamma(\mathbf{r}) + k^2\Gamma(\mathbf{r}) = \delta(\mathbf{r})$:

$$\begin{aligned}\mathbf{E}_1(\mathbf{r}) &= -4\pi k^2 \int \mathrm{d}^3\mathbf{r}'\, \Gamma(\mathbf{r}-\mathbf{r}')\, \mathbf{P}(\mathbf{r}') \\ &= k^2 \int \mathrm{d}^3\mathbf{r}'\, \frac{\exp(\mathrm{i}k|\mathbf{r}-\mathbf{r}'|)}{|\mathbf{r}-\mathbf{r}'|}\, \mathbf{P}(\mathbf{r}').\end{aligned} \tag{28}$$

Recalling that $\boldsymbol{\mathcal{E}}_1 = \mathrm{Re}\,\mathbf{E}_1$ and substituting (28) into (25), we obtain the following expression for the contribution δu_r of one particle to the detected signal:

$$\begin{aligned}\delta u_r = \frac{2k^2}{T}\,\mathrm{Re}\int_0^T \mathrm{d}t \int \mathrm{d}^3\mathbf{r}' \big\{ &\cos[2\phi]\big(\Phi_x(\mathbf{r}')P_x(\mathbf{r}') \\ &- \Phi_z(\mathbf{r}')\,P_z(\mathbf{r}')\big) - \sin[2\phi]\big(\Phi_x(\mathbf{r}')\,P_z(\mathbf{r}') + \Phi_z(\mathbf{r}')\,P_x(\mathbf{r}')\big)\big\},\end{aligned} \tag{29}$$

where

$$\begin{aligned}\Phi_i(\mathbf{r}') &\equiv \int_S \mathrm{d}x\,\mathrm{d}z\; \mathcal{E}_{0i}(x,y,z,t)\; \frac{\exp(\mathrm{i}k|\mathbf{r}-\mathbf{r}'|)}{|\mathbf{r}-\mathbf{r}'|}\bigg|_{y=L} \\ &\equiv \Phi_i^+(\mathbf{r}')\exp(-\mathrm{i}\omega t) + \Phi_i^-(\mathbf{r}')\exp(\mathrm{i}\omega t),\ i = x, z.\end{aligned} \tag{30}$$

Here, $\mathbf{r} \equiv (x,y,z)$ and L determines the position of the plane of the surface S of photodetectors, over which the integration in Eqn (25) is performed (see Fig. 1). The polarization $\mathbf{P}(\mathbf{r}')$ (26) depends on time as $\exp(-\mathrm{i}\omega t)$; therefore, after averaging over time, only the component Φ_i^- of function Φ_i will enter the expression for the detected signal. We present the results of calculating this component for the case when the probe beam is a linearly polarized *Gaussian* beam with the polarization azimuth θ, propagating in the direction of the y-axis and having a waist at $y = 0$. The complex electric field of such a beam has the form [25]

$$\begin{aligned}\mathbf{E}_0(\mathbf{r}) = \exp\big[\mathrm{i}(ky-\omega t)\big]\sqrt{\frac{8W}{c}}\,\frac{kQ}{2k+\mathrm{i}Q^2 y} \\ \times \exp\left[-\frac{kQ^2(x^2+z^2)}{2(2k+\mathrm{i}Q^2 y)}\right]\mathbf{D} \equiv \mathcal{A}_0(\mathbf{r})\;\mathbf{D}\exp-(\mathrm{i}\omega t), \\ \mathbf{D} = \begin{pmatrix}\sin\theta \\ 0 \\ \cos\theta\end{pmatrix},\end{aligned} \tag{31}$$

where $\mathbf{r} = (x,y,z)$, and the parameter Q is defined as $Q \equiv 2/\rho_\mathrm{c}$, where ρ_c is the e-level radius of the beam waist (caustic). The polarization of the beam is determined by the unit Jones vector $\mathbf{D}$ having only x and y components in the present case.[16] The calculation of the components Φ_i^- for a Gaussian beam (31) given in the Appendix yields the following result [58]:

$$\begin{pmatrix}\Phi_x^-(\mathbf{r}') \\ \Phi_z^-(\mathbf{r}')\end{pmatrix} = -\mathbf{D}\,\frac{\mathrm{i}\pi}{k}\;\mathcal{A}_0^*(\mathbf{r}'), \quad |\mathbf{r}'| \ll L, \tag{32}$$

where $\mathcal{A}_0^*(\mathbf{r}')$ is determined from Eqn (31). Substituting Eqns (26) and (32) into Eqn (29), we arrive at the following expression for the contribution of the considered particle to the polarimetric signal: $\delta u_r = 2\pi k\ \mathrm{Im}\ \mathcal{A}^*(\mathbf{R})\{\langle d_x\rangle \sin[\theta - 2\phi] - \langle d_z\rangle \cos[\theta - 2\phi]\}$.

In the above calculation, we considered the polarimetric detector to be operating in the Faraday rotation detection mode, when *5* in Fig. 1 is a half-wave phase plate, its rotation corresponding to the change in angle ϕ. Let us now take into account that in a real experiment the polarimetric detector is always *balanced* to compensate for excess noise. For this purpose, the angle ϕ is chosen such that the output signal U of the detector, illuminated only by the probe beam $\mathbf{E}_0$, turns into zero.[17] If, as we considered above, the probe beam is linearly polarized, this means that $\phi = \theta + \pi/4$ (see Eqn (24), where $\boldsymbol{\mathcal{E}} \to \mathbf{E}_0$ is determined in Eqn (31)) and, therefore, the signal of Faraday rotation from one particle, recorded by the balanced detector, is expressed as $\delta u_r = 2\pi k\ \mathrm{Im}\ \mathcal{A}^*(\mathbf{R})[\langle d_z\rangle \sin\theta - \langle d_x\rangle \cos\theta]$.

Now, we consider the case where the polarimetric detector operates in the ellipticity detection mode. To transit to this mode, a quarter-wave phase plate is installed as *5*, which is oriented so that its axes form an angle of $\pi/4$ with the principal directions of the polarizing beam splitter *6*. It can be verified that, with an arbitrarily oriented *linearly* polarized input optical beam, the output signal of the detector, operating in this mode, is zero and appears only if the polarization of the input beam becomes elliptic. As a result of calculations like those presented above, it turns out that the expression for the ellipticity signal from one particle (we denote it by δu_e) differs from the expression for δu_r only by replacing symbol Im with symbol Re. Hence, the signals δu_r and δu_e can be presented in a compact form as an imaginary and real part of one complex signal δu determined by the relation

$$\begin{aligned}\delta u = \delta u_e + \mathrm{i}\delta u_r &= 2\pi k\ \mathcal{A}^*(\mathbf{R})\big(\langle d_z\rangle \sin\theta - \langle d_x\rangle \cos\theta\big) \\ &= 2\pi k\ \mathcal{A}^*(\mathbf{R})[\mathbf{d}\times\mathbf{D}]_y.\end{aligned} \tag{33}$$

[15] The presence of this term follows from Maxwell's equations.

[16] This is a consequence of the electromagnetic wave transversity. We ignore the polarization change at the beam edges.

[17] In this case, the occurrence of the output signal is related to the scattered field $\mathbf{E}_1$.

In correspondence with the above assumptions, the vector **d** of the particle dipole moment can be expressed in terms of the probe beam field strength amplitude using the polarizability tensor α of the considered particle (atom, ion): $d_i = \mathcal{A}(\mathbf{R})\alpha_{ik}D_k$. Under typical SNS experimental conditions, the studied sample particles are not externally excited and are in the quantum state which is a random linear combination of the stationary states split by the magnetic field. Such a *superposition* state is nonstationary and necessarily time dependent, the characteristic frequencies of this dependence being determined by the magnetic splitting frequencies mentioned above. In turn, this leads to the time dependence of the tensor α and the polarimetric signal δu recorded in SNS.

The calculation of time dependence of the polarimetric signal is seen to reduce to the calculation of time-dependent susceptibility (the polarizability tensor) of the sample particles in a superposition state. The general character of such calculations is illustrated by the case where such particles are atoms, in which the ground energy level in a zero magnetic field is a multiplet with the total angular momentum F (i.e., a set of $2F+1$ states $\mathbf{B}=0$ degenerate at $|M\rangle$ with the projection $\hbar M$ of the angular momentum on the z-axis, $M=-F, 1-F, \ldots, F$). Let us choose one of these atoms and consider it at the time instant when it enters the probe beam (let this instant be $t=0$). Assume that the energy distance to the nearest excited state of the considered atom is so large that the atomic wave function $|\Psi(t=0)\rangle = |\Psi(0)\rangle$ can be represented by a linear combination of the states belonging to the considered multiplet only, $|\Psi(0)\rangle = \sum_{M=-F}^{F} C_M(0)|M\rangle$, where $C_M(0)$ are random complex numbers, and $\sum_{M=-F}^{F}|C_M(0)|^2 = 1$. The matrix H_B of the interaction Hamiltonian of the atom with the external magnetic field **B** in the representation of wave functions of the ground atomic multiplet $|M\rangle$, $M=-F,\ldots,F$, has the form $H_B = \hbar^{-1} g_L \beta (\mathbf{B}, \mathbf{J}) \equiv (\boldsymbol{\Omega}_\mathrm{L}, \mathbf{J})$, where $J_{x,y,z}$ are the known matrices of the angular momentum projection operators [76], and g_L is the Lande factor of the considered multiplet. The atomic wave function satisfies the Schrödinger equation $\mathrm{i}\dot{\Psi} = H_B\Psi$; therefore, $\Psi(t) = \exp(-\mathrm{i}H_B t)\Psi(0)$. Since $\exp(-\mathrm{i}H_B t) = \exp(-(\boldsymbol{\Omega}_\mathrm{L}, \mathbf{J})t)$ is the operator of spatial rotation around vector $\boldsymbol{\Omega}_\mathrm{L}$ by the angle $\Omega_\mathrm{L} t$ [76], the dynamics of the wave function in our case consist of its spatial rotation around the magnetic field direction with the Larmor frequency Ω_L. Similar rotation is experienced by all quantities related to the wave function. For example, the magnetic moment vector of the atom $\mu = g_L\beta\langle\Psi|\mathbf{J}|\Psi\rangle$ rotates around the magnetic field with the Larmor frequency. In the linear response theory, the polarizability tensor α interesting for us is also determined by the atomic wave function $|\Psi(t)\rangle$ (or the appropriate density matrix). Therefore, in the measurement of the atomic wave function described above, the atomic polarizability tensor experiences the transformation, equivalent to a rotation of the coordinate system around the magnetic field with the Larmor frequency. With some simplifications, this transformation can be thought of as follows.

If the studied atomic system is transparent to the probe beam, then the tensor α can be considered Hermitian in a reasonable approximation $\alpha_{ik} = \alpha_{ki}^*$ and be written as the sum of a real symmetric part and an imaginary antisymmetric part, $\alpha = \alpha^s + \alpha^a$, where $\alpha_{ik}^{s(a)} \equiv [\alpha_{ik} + (-)\alpha_{ki}]/2$. Using the Levi–Civita symbol ε_{ikj}, a real *gyration* vector α^a [77] can be put into correspondence to the imaginary antisymmetric part **G**: $\alpha_{ik}^a = \mathrm{i}\varepsilon_{ikj}G_j$. The real tensor α^s can be completely described by its principal values and the positions of the principal axes. With these simplifications, the above dynamics of the atomic polarizability tensor can be presented by a rotation of the gyration vector **G** and the principal axes of the tensor α^s around the magnetic field with the Larmor frequency Ω_L. Note here that, since all vectors determined by the superposition wave function of a multiplet with the given total angular momentum are proportional to each other, the gyration vector **G** introduced above is proportional to the magnetization vector μ which we used in previous sections to describe the contributions of sample particles to the Faraday rotation signal.

Equation (33) written in terms of the symmetric tensor α^s and gyration vector **G** takes the form

$$\delta u = 2\pi k\left|\mathcal{A}(\mathbf{R})\right|^2\left([\alpha^s\,\mathbf{D}\times\mathbf{D}]_y + \mathrm{i}G_y\right) = 2\pi k\left|\mathcal{A}(\mathbf{R})\right|^2 \times\left[\frac{\alpha_{zz}^s - \alpha_{xx}^s}{2}\sin(2\theta) - \alpha_{zx}^s\cos(2\theta) + \mathrm{i}G_y\right]. \quad (34)$$

4.3 Basic configurations of the experiment

Using the above formula, let us analyze two base geometries of an experiment on optical detection of spin fluctuations.

In the first of them, the Voigt geometry (typical of SNS), the Faraday rotation noise is observed, the magnetic field being oriented along the z-axis perpendicular to the probe beam (see Fig. 1). In such a setting of the experiment, from each particle only the imaginary part of the polarimetric signal $\delta u_r = 2\pi k\,|\mathcal{A}(\mathbf{R})|^2 G_y(t)$, related to the y projection of the gyration vector, is recorded. Since in this case the gyration vector of each particle rotates around the z-axis with the Larmor frequency Ω_L, its projection G_y harmonically oscillates at the same frequency. Therefore, the Faraday rotation noise observed in this geometry will be spectrally localized at the Larmor frequency Ω_L. As was indicated above, the gyration vector is proportional to the magnetization vector used in the previous sections to describe such an experiment; therefore, the considered case confirms the analysis presented in these sections from the point of view of scattering theory.

Now, let us consider an alternative geometry of SNS, called the *Faraday geometry*, when the magnetic field is directed parallel to the probe beam, and the polarimetric detector operates in the ellipticity detection mode. In this case, only the real part $\delta u_e = 2\pi k\,|\mathcal{A}(\mathbf{R})|^2 \times [\alpha^s(t)\,\mathbf{D}\times\mathbf{D}]_y$ of the polarimetric signal is recorded from every particle. As was mentioned above, the time dependence of the tensor α^s corresponds to a rotation of its principal axes around the y-axis, along which in this case the magnetic field is directed. We denote by $Y(\phi)$ the matrix of coordinate transformation for the coordinate system rotation by the angle ϕ around the y-axis. Then, $\alpha^s(t) = Y(-\Omega_\mathrm{L}t)\alpha(0)Y(\Omega_\mathrm{L}t)$. Since the y projection of a vector product of any two vectors **A** and **B** remains unchanged under such a transformation, $[\mathbf{A}\times\mathbf{B}]_y = [Y(\Omega_\mathrm{L}t)\mathbf{A}\times Y(\Omega_\mathrm{L}t)\,\mathbf{B}]_y$, we can write for the recorded ellipticity signal δu_e the following chain of equalities:

$$\delta u_e = 2\pi k\left|\mathcal{A}(\mathbf{R})\right|^2\left[Y(-\Omega_\mathrm{L}t)\,\alpha^s(0)\,Y(\Omega_\mathrm{L}t)\,\mathbf{D}\times\mathbf{D}\right]_y = 2\pi k\left|\mathcal{A}(\mathbf{R})\right|^2\left[\alpha^s(0)\,Y(\Omega_\mathrm{L}t)\,\mathbf{D}\times\,Y(\Omega_\mathrm{L}t)\,\mathbf{D}\right]_y. \quad (35)$$

This chain shows that the transformation of the polarizability tensor α^s in this case is equivalent to the rotation of the Jones

vector **D** of the probe beam around the y-axis through the angle $\Omega_L t$. Such a rotation corresponds to the change $\theta \to \theta + \Omega_L t$ in expression (31) for the vector **D**:

$$Y(\Omega_L t)\,\mathbf{D} = \begin{pmatrix} \sin[\theta + \Omega_L t] \\ 0 \\ \cos[\theta + \Omega_L t] \end{pmatrix}. \quad (36)$$

Thus, the expression for the polarimetric signal δu_e observed in the Faraday geometry can be obtained by performing the change $\theta \to \theta + \Omega_L t$, $\alpha^s_{ik} \to \alpha^s_{ik}(0)$ in Eqn (34) and keeping only the real part of the quantity δu:

$$\delta u_e = 2\pi k \left|\mathcal{A}(\mathbf{R})\right|^2 \left[\frac{\alpha^s_{zz}(0) - \alpha^s_{xx}(0)}{2} \sin\left[2(\theta + \Omega_L t)\right] - \alpha^s_{zx}(0) \cos\left[2(\theta + \Omega_L t)\right]\right]. \quad (37)$$

From the last formula, it is seen that in the Faraday geometry the contribution of every particle oscillates in time at the *doubled* Larmor frequency $2\Omega_L$, due to which the ellipticity noise recorded in this geometry turns out to be spectrally localized at the frequency $2\Omega_L$, as it was in experiment [26], described in the previous section.

Thus, it turns out possible to substantiate the simplified picture of polarimetric noise formation used in the previous Sections from the point of view of the scattering theory.

To finalize this section, we note that the power spectra of polarimetric noise recorded in the SNS, strictly speaking, are determined by the Fourier transforms of the correlation functions $\langle \delta u_r(t) \delta u_r(0) \rangle$ and $\langle \delta u_e(t) \delta u_e(0) \rangle$, the calculation of which requires considering the relaxation processes and constructing a specified model of moving the sample particles through the probe beam. Such calculations are performed in Refs [25, 26].

5. Conclusions

The spectroscopy of spin fluctuations is one of the rare cases where the content of the fluctuation-dissipation theorem is used directly, implying the possibility of extracting the spectrum of the system's linear susceptibility from the spectrum of its spontaneous noise. Studies of the spectra of luminescence or other spontaneous emission from objects can in part be considered noise measurements of this kind. However, only in two methods of spectroscopy, spin noise spectroscopy and EPR spectroscopy, do these two approaches meet in such a refined form. The experimental comparison of these approaches made it possible for the first time to compare their capabilities and to reveal several interesting features of the magnetic resonance noise technique. Of course, it is necessary to bear in mind that the noise technique in the implemented form uses an *optical method* of detecting the magnetization, which substantially enriches its capabilities. The achievements of SNS have shown that, using stochastic signals, regardless of their statistically small value in macroscopic samples (compared to regular response signals), it is possible to implement a quite practical method of investigating the susceptibility spectrum and internal dynamics of a medium.

The prospects of further development of the SNS method are determined by the variety of its possible applications in radio spectroscopic and optical studies of paramagnetic media, as well as by the continuously growing significance of spin degrees of freedom in the devices of modern photonics and informatics. In recent times, the scope of SNS objects has been substantially extended; along with atomic and semiconductor systems, which can already be called classical SNS objects, it includes dielectrics with impurity paramagnetic ions, and the potentiality of applying this technique to subjects with weakly allowed optical transitions has been demonstrated. The information capabilities of multibeam SNS methods are under intense research. With further development of this research field and clarifying its informative potential, the issues of correct theoretical description of SNS signal formation in media with various kinematics of spin carriers under various conditions of medium probing and various configurations of measurement setup will become more and more important. This is exactly why so much attention in this review was paid to rigorous solutions to basic SNS problems in the model of inelastic light scattering.

Acknowledgments. This review was prepared with financial support from the Russian Science Foundation, grant no. 21-72-10021. A V Kavokin expresses gratitude to Saint Petersburg State University (SPSU) (grant no. 95442589) for the support for theoretical studies that grounded Section 3.9. The studies of halogenide perovskites (Section 3.4) were carried out with support from the Ministry of Science and Higher Education of the Russian Federation within the framework of Megagrant No. 075-15-2022-1112. The presented experimental results, except those in Fig. 5, were obtained at the facilities of the Nanophotonics Center of the SPSU Research Park.

6. Appendix

Let us calculate the function Φ_i^- (Eqn (30)). We introduce the following auxiliary functions: $\mathbf{F}(\mathbf{r}') \equiv \int_S \mathrm{d}x\,\mathrm{d}z\,\mathbf{E}_0(\mathbf{r}) \Gamma(\mathbf{r}-\mathbf{r}') \sim \exp(-\mathrm{i}\omega t)$ and $\mathbf{P}(\mathbf{r}') \equiv \int_S \mathrm{d}x\,\mathrm{d}z \times \mathbf{E}_0^*(\mathbf{r}) \Gamma(\mathbf{r}-\mathbf{r}') \sim \exp(\mathrm{i}\omega t)$, depending on time, respectively, as $\exp(-\mathrm{i}\omega t)$ and $\exp(\mathrm{i}\omega t)$ (see Eqn (31)). Then, it is not difficult to see that $\Phi_\alpha(\mathbf{r}') = -2\pi[F_\alpha(\mathbf{r}') + P_\alpha(\mathbf{r}')]$ and, therefore, $\Phi_\alpha^-(\mathbf{r}') \exp(\mathrm{i}\omega t) = -2\pi P_\alpha(\mathbf{r}')$. To calculate the integral in the expression for $P_\alpha(\mathbf{r}')$, we use the Kirchhoff formula for the field:

$$\mathbf{E}_0^*(\mathbf{R}) = \int_{\partial V} \left[\mathbf{E}_0^*(\mathbf{r}) \frac{\partial \Gamma(\mathbf{r}-\mathbf{R})}{\partial n} - \Gamma(\mathbf{r}-\mathbf{R}) \frac{\partial \mathbf{E}_0^*(\mathbf{r})}{\partial n}\right] \mathrm{d}S. \quad (38)$$

Here, ∂V is an arbitrary closed surface enclosing the point **R**, and the symbol $\partial/\partial n$ denotes a derivative along the normal to the surface ∂V. For definiteness, we assume that the photosensitive surface S of the photodetectors is larger than the 'section' of the probe Gaussian beam, so that the photodetectors 'catch' practically all the flow of its energy (recall that S is in the plane $y = L \gg |\mathbf{R}|$). In addition, we assume that the size of the surface S (we denote it as $\sqrt{S}$) is substantially smaller than the distance L from the scattering particle to the photodetectors, $\sqrt{S} \ll L$. We now choose the surface ∂V in the form of a cylinder whose axis is parallel to the y-axis, resting on the surface S ($y = L$) on the right and on the surface S' ($y = -L$ symmetric to it with respect to the origin of coordinates on the left (Fig. 11)).

Since the probe beam is inside the cylinder constructed in such a way, the integral in the Kirchhoff form (38) can be calculated only over the surfaces S and S' — on the side surface of the cylinder the probe beam field strength is

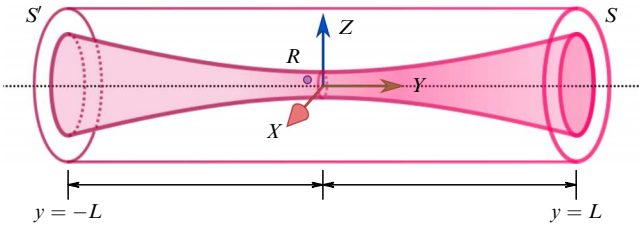

Figure 11. See explanation in the text.

negligibly small. Both surfaces are perpendicular to the y-axis and have oppositely directed normal vectors; therefore, on the surface S the normal derivative is calculated as $\partial/\partial n \to \partial/\partial y$, and on the surface S', as $\partial/\partial n \to -\partial/\partial y$. We calculate the derivative of the Green's function $\partial\Gamma(\mathbf{r}-\mathbf{R})/\partial n$ on the surface S (i.e., at $y = L$):

$$\left.\frac{\partial\Gamma(\mathbf{r}-\mathbf{R})}{\partial n}\right|_S = \frac{\partial\Gamma(\mathbf{r}-\mathbf{R})}{\partial y} = \frac{\partial\Gamma(\mathbf{r}-\mathbf{R})}{\partial|\mathbf{r}-\mathbf{R}|}\,\frac{\partial|\mathbf{r}-\mathbf{R}|}{\partial y}$$

$$= \frac{\partial\Gamma(\mathbf{r}-\mathbf{R})}{\partial|\mathbf{r}-\mathbf{R}|}\,\frac{y-R_y}{|\mathbf{r}-\mathbf{R}|}$$

$$= \Gamma(\mathbf{r}-\mathbf{R})\left[\mathrm{i}k - \underbrace{\frac{1}{|\mathbf{r}-\mathbf{R}|}}_{\approx L^{-1}\ll k}\right]\underbrace{\frac{L-R_y}{|\mathbf{r}-\mathbf{R}|}}_{\approx 1} \approx \mathrm{i}k\Gamma(\mathbf{r}-\mathbf{R})\,. \tag{39}$$

The approximations used are justified because $R, \sqrt{S} \ll L$ ($R \equiv |\mathbf{R}|$) and, therefore, $|L-R_y|, |\mathbf{r}-\mathbf{R}| \sim L$. This allows ignoring the second term in the square brackets, since $|\mathbf{r}-\mathbf{R}|^{-1} \sim L^{-1} \ll k = 2\pi/\lambda$. Moreover, the factor $[y-R_y]/|\mathbf{r}-\mathbf{R}|$ at $r, y \gg R$ is practically equal to that on the surface S. The Green's function derivative $\partial\Gamma(\mathbf{r}-\mathbf{R})/\partial n$ on the surface S' (i.e., at $y = -L$) is calculated similarly:

$$\left.\frac{\partial\Gamma(\mathbf{r}-\mathbf{R})}{\partial n}\right|_{S'} = -\frac{\partial\Gamma(\mathbf{r}-\mathbf{R})}{\partial y} = -\frac{\partial\Gamma(\mathbf{r}-\mathbf{R})}{\partial|\mathbf{r}-\mathbf{R}|}\,\frac{\partial|\mathbf{r}-\mathbf{R}|}{\partial y}$$

$$= -\frac{\partial\Gamma(\mathbf{r}-\mathbf{R})}{\partial|\mathbf{r}-\mathbf{R}|}\,\frac{y-R_y}{|\mathbf{r}-\mathbf{R}|}$$

$$= -\Gamma(\mathbf{r}-\mathbf{R})\left[\mathrm{i}k - \underbrace{\frac{1}{|\mathbf{r}-\mathbf{R}|}}_{\approx L^{-1}\ll k}\right]\underbrace{\frac{-L-R_y}{|\mathbf{r}-\mathbf{R}|}}_{\approx -1}$$

$$\approx \mathrm{i}k\Gamma(\mathbf{r}-\mathbf{R})\,. \tag{40}$$

Thus, we conclude that on both surfaces S and S' the relation is valid:

$$\frac{\partial\Gamma(\mathbf{r}-\mathbf{R})}{\partial n} = \mathrm{i}k\Gamma(\mathbf{r}-\mathbf{R})\,. \tag{41}$$

We now proceed to the calculation of the derivative $\partial\mathbf{E}_0^*(\mathbf{r})/\partial n$ that enters Eqn (38). First, we calculate it on the surface S, where $\partial/\partial n = \partial/\partial y$. In this case, in the expression for $\mathbf{E}_0^*(\mathbf{r})$ that follows from (31), we take into account only the first exponential factor, because it most strongly depends on y. The dependence on y of the rest of the factors describing the field oscillation amplitude distribution in the probe beam can be ignored if the Rayleigh length of the beam $\sim \rho_c^2/\lambda$ substantially exceeds the wavelength λ (which is commonly so). Keeping this in mind, we obtain

$$\left.\frac{\partial\mathbf{E}_0^*(\mathbf{r})}{\partial n}\right|_S = \frac{\partial\mathbf{E}_0^*(\mathbf{r})}{\partial y} = -\mathrm{i}k\mathbf{E}_0^*(\mathbf{r})\,. \tag{42}$$

A similar calculation of the derivative $\partial\mathbf{E}_0^*(\mathbf{r})/\partial n$ on the surface S' leads to the expression

$$\left.\frac{\partial\mathbf{E}_0^*(\mathbf{r})}{\partial n}\right|_{S'} = -\frac{\partial\mathbf{E}_0^*(\mathbf{r})}{\partial y} = \mathrm{i}k\mathbf{E}_0^*(\mathbf{r})\,. \tag{43}$$

Substituting the obtained relations into Eqn (38), we get

$$\mathbf{E}_0^*(\mathbf{R}) = \int_S \left[\mathbf{E}_0^*(\mathbf{r})\,\frac{\partial\Gamma(\mathbf{r}-\mathbf{R})}{\partial n} - \Gamma(\mathbf{r}-\mathbf{R})\,\frac{\partial\mathbf{E}_0^*(\mathbf{r})}{\partial n}\right]\mathrm{d}S$$

$$+ \underbrace{\int_{S'} \left[\mathbf{E}_0^*(\mathbf{r})\,\frac{\partial\Gamma(\mathbf{r}-\mathbf{R})}{\partial n} - \Gamma(\mathbf{r}-\mathbf{R})\,\frac{\partial\mathbf{E}_0^*(\mathbf{r})}{\partial n}\right]\mathrm{d}S}_{=0}$$

$$= 2\mathrm{i}k\int_S \mathbf{E}_0^*(\mathbf{r})\Gamma(\mathbf{r}-\mathbf{R})\,\mathrm{d}S = 2\mathrm{i}k\,\mathbf{P}(\mathbf{R})\,. \tag{44}$$

Recalling that $\Phi_\alpha^-(\mathbf{r}')\exp(\mathrm{i}\omega t) = -2\pi P_\alpha(\mathbf{r}')$, we get

$$E_{0\alpha}^*(\mathbf{R}) = -\frac{\mathrm{i}k}{\pi}\,\Phi_\alpha^-(\mathbf{R})\exp(\mathrm{i}\omega t)\,, \tag{45}$$

from which, using Eqn (31), we obtain the result (32).

References

1. Kubo R *Statistical Mechanics* (Amsterdam: North-Holland, 1965); Translated into Russian: *Statisticheskaya Mekhanika* (Translated Ed. by N D Zubarev) (Moscow: Mir, 1967)
2. Sleator T et al. *Phys. Rev. Lett.* **55** 1742 (1985)
3. Sleator T et al. *Phys. Rev. B* **36** 1969 (1987)
4. McCoy M A, Ernst R R *Chem. Phys. Lett.* **159** 587 (1989)
5. Guéron M, Leroy J L *J. Magn. Reson. 1969* **85** 209 (1989)
6. Müller N, Jerschow A *Proc. Natl. Acad. Sci. USA* **103** 6790 (2006)
7. Aleksandrov E B, Zapasskii V S *Sov. Phys. JETP* **54** 64 (1981); *Zh. Eksp. Teor. Fiz.* **81** 132 (1981)
8. Müller G M et al. *Physica E* **43** 569 (2010)
9. Zapasskii V S *Adv. Opt. Photon.* **5** 131 (2013)
10. Hübner J et al. *Phys. Status Solidi B* **251** 1824 (2014)
11. Sinitsyn N A, Pershin Yu V *Rep. Prog. Phys.* **79** 106501 (2016)
12. Glazov M M *J. Exp. Theor. Phys.* **122** 472 (2016); *Zh. Eksp. Teor. Fiz.* **149** 547 (2016)
13. Zapasskii V S, Kozlov G G *Phys. Usp.* **60** 628 (2017); *Usp. Fiz. Nauk* **187** 675 (2017)
14. Aleksandrov E B et al. *Sov. Phys. Usp.* **26** 643 (1983); *Usp. Fiz. Nauk* **140** 547 (1983)
15. Weil J A, Bolton J R *Electron Paramagnetic Resonance: Elementary Theory and Practical Applications* 2nd ed. (Hoboken, NJ: Wiley-Interscience, 2007)
16. Poltavtsev S V et al. *Phys. Rev. B* **89** 081304 (2014)
17. Dahbashi R et al. *Phys. Rev. Lett.* **112** 156601 (2014)
18. Ryzhov I I et al. *Appl. Phys. Lett.* **106** 242405 (2015)
19. Ryzhov I I et al. *Sci. Rep.* **6** 21062 (2016)
20. Ryzhov I I et al. *J. Appl. Phys.* **117** 224305 (2015)
21. Mitsui T *Phys. Rev. Lett.* **84** 5292 (2000)
22. Zapasskii V S et al. *Phys. Rev. Lett.* **110** 176601 (2013)
23. Yang L et al. *Nat. Commun.* **5** 4949 (2014)
24. Glazov M M, Zapasskii V S *Opt. Express* **23** 11713 (2015)
25. Kozlov G G, Ryzhov I I, Zapasskii V S *Phys. Rev. A* **95** 043810 (2017)
26. Fomin A A et al. *Phys. Rev. Res.* **2** 012008 (2020)
27. Kamenskii A N et al. *Phys. Rev. Res.* **2** 023317 (2020)
28. Smirnov D S, Mantsevich V N, Glazov M M *Phys. Usp.* **64** 923 (2021); *Usp. Fiz. Nauk* **191** 973 (2021)
29. Kamenskii A N et al. *Phys. Rev. B* **105** 014416 (2022)

30. Kozlov V O et al. *Phys. Rev. B* **107** 064427 (2023)
31. Zapasskii V S *J. Appl. Spectrosc.* **37** 857 (1982); *Zh. Priklad. Spektrosk.* **37** 181 (1982)
32. Kozlov G G, Ryzhov I I, Zapasskii V S *Phys. Rev. A* **97** 013848 (2018)
33. Kharkevich A A *Spectra and Analysis* (New York: Consultants Bureau, 1960); Translated from Russian: *Spektry i Analiz* (Moscow: Librokom, 2009)
34. Forrester A T, Gudmundsen R A, Johnson P O *Phys. Rev.* **99** 1691 (1955)
35. Abragam A *The Principles of Nuclear Magnetism* (Oxford: Clarendon Press, 1961); Translated into Russian: *Yadernyi Magnetizm* (Translated Ed. by G V Skrotskii) (Moscow: IL, 1963)
36. Römer M, Hübner J, Oestreich M *Rev. Sci. Instrum.* **78** 103903 (2007)
37. Römer M et al. *Phys. Rev. B* **81** 075216 (2010)
38. Crooker S A et al. *Phys. Rev. Lett.* **104** 036601 (2010)
39. Müller G M et al. *Appl. Phys. Lett.* **97** 192109 (2010)
40. Oestreich M et al. *Phys. Rev. Lett.* **95** 216603 (2005)
41. Weisbuch C, Vinter B *Quantum Semiconductor Structures*: *Fundamentals and Applications* (Boston, MA: Academic Press, 1991)
42. Fleisher V G, Merkulov I A "5. Optical orientation of the coupled electron-nuclear spin system of a semiconductor," in *Optical Orientation* (Modern Problems in Condensed Matter Sciences, Vol. 8, Eds F Meier, B P Zakharchenya) (Amsterdam: North-Holland, 1984) p. 173
43. van der Ziel J P, Pershan P S, Malmstrom L D *Phys. Rev. Lett.* **15** 190 (1965)
44. Battiato M, Barbalinardo G, Oppeneer P M *Phys. Rev. B* **89** 014413 (2014)
45. Buckingham A D, Stephens P J *Annu. Rev. Phys. Chem.* **17** 399 (1966)
46. Petrov M Yu et al. *Phys. Rev. A* **97** 032502 (2018)
47. Zapasskii V S *Phys. Solid State* **61** 847 (2019); *Fiz. Tverd. Tela* **61** 946 (2019)
48. Kozlov V O et al. *J. Non-Cryst. Solids* **621** 122610 (2023)
49. Kozlov V O et al. *Phys. Rev. Lett.* **129** 077401 (2022)
50. Shumitskaya A A et al. *Adv. Opt. Mater.* 2302095 (2023) https://doi.org/10.1002/adom.202302095
51. Kozlov V O et al. "Spin noise of a halide perovskite," arXiv:2311.06077
52. Römer M, Hübner J, Oestreich M *Appl. Phys. Lett.* **94** 112105 (2009)
53. Müller G M et al. *Phys. Rev. B* **81** 121202 (2010)
54. Berski F et al. *Phys. Rev. Lett.* **111** 186602 (2013)
55. Hübner J et al. *Opt. Express* **21** 5872 (2013)
56. Petrov M Yu et al. *Phys. Rev. B* **97** 125202 (2018)
57. Cronenberger S et al. *Phys. Rev. Lett.* **123** 017401 (2019)
58. Kozlov G G, Zapasskii V S, Shapochkin P Yu *Appl. Opt.* **57** B170 (2018)
59. Sterin P et al. *Phys. Rev. Appl.* **9** 034003 (2018)
60. Kozlov G G et al. *Phys. Rev. A* **98** 043810 (2018)
61. Ryzhov I I et al. *Phys. Rev. B* **93** 241307 (2016)
62. Wertz E et al. *Appl. Phys. Lett.* **95** 051108 (2009)
63. Schneider C et al. *Nature* **497** 348 (2013)
64. Read D et al. *Phys. Rev. B* **80** 195309 (2009)
65. Glazov M M et al. *Phys. Rev. B* **88** 041309 (2013)
66. Baumberg J J et al. *Phys. Rev. Lett.* **101** 136409 (2008)
67. Levrat J et al. *Phys. Rev. Lett.* **104** 166402 (2010)
68. Balas Y C et al. *Phys. Rev. Lett.* **128** 117401 (2022)
69. Tsotsis P et al. *New J. Phys.* **14** 023060 (2012)
70. Christopoulos S et al. *Phys. Rev. Lett.* **98** 126405 (2007)
71. Cristofolini P et al. *Phys. Rev. Lett.* **110** 186403 (2013)
72. Pickup L et al. *Phys. Rev. B* **103** 155302 (2021)
73. Ryzhov I I et al. *Phys. Rev. Res.* **2** 022064 (2020)
74. Shelykh I et al. *Phys. Rev. B* **70** 115301 (2004)
75. Gorbovitskii B M, Perel V I *Opt. Spectrosc.* **54** 229 (1983); *Opt. Spektrosk.* **54** 388 (1983)
76. Landau L D, Lifshitz E M *Quantum Mechanics*: *Non-Relativistic Theory* (Oxford: Pergamon Press, 1981); Translated from Russian: *Kvantovaya Mekhanika* (*Nerelyativistskaya Teoriya*) 6th ed., revised (Moscow: Fizmatlit, 2004)
77. Landau L D, Lifshitz E M *Electrodynamics of Continuous Media* (Oxford: Pergamon Press, 1984); Translated from Russian: *Elektrodinamika Sploshnykh Sred* (Moscow: Fizmatlit, 2005) p. 30